Received: 6 May 2021 | Revised: 25 March 2022 | Accepted: 21 May 2022

DOI: 10.33012/navi.532

ORIGINAL ARTICLE

The Role of Antennas on GNSS Pseudorange and Multipath Errors and Their Impact on DFMC Multipath Models for Avionics

Stefano Caizzone[1] | **Mihaela-Simona Circiu**[1] | **Wahid Elmarissi**[1] | **Christoph Enneking**[1] | **Markus Rippl**[1] | **Matteo Sgammini**[2]

[1]Institute of Communications and Navigation, German Aerospace Center (DLR)

[2]European Commission, Joint Research Centre (JRC), Ispra, Italy

Abstract

Current satellite navigation systems are providing more and more dual-frequency capabilities, enabling improved navigation accuracy and a reduction of residual errors (e.g., from ionosphere). Recently, the aviation community has started an effort to achieve new standardized Minimum Operational Performance Specifications (MOPS) for GNSS equipment in order to allow for the use of dual-frequency multi-constellation (DFMC) systems in the future, with clear benefits in terms of obtainable navigation performance. In such conditions, residual errors introduced by the user GNSS antenna become even more relevant and need to be properly identified and bounded, both in antenna specifications and in the models for aircraft multipath. The present work investigates this problem and shows the results of an activity aiming at new airborne multipath models for L1/E1 and L5/E5a frequency bands and for their ionospheric-free combination. The paper outlines a detailed investigation of the physical rationale of such errors.

Keywords

airborne error model, GNSS antenna, group delay variation, multipath, multipath rejection

1 | INTRODUCTION

In the quest for the optimal exploitation of the benefits of dual-frequency multi-constellation (DFMC) systems, the aviation community has committed to the development of new avionics standards for the GNSS equipment flown on commercial aircraft. Such efforts also open the possibility to more deeply analyze certain phenomena by taking advantage of modern simulation tools that were not available or were only partially available at the time that single-frequency models were first defined. With the removal of first-order ionospheric errors due to dual-frequency pseudorange measurement combinations, the remaining user errors (noise, antenna, multipath) become more relevant and are the dominant error sources that have to be addressed and properly bounded for performance-based navigation (Circiu et al., 2017; Salabert, 2015).

In this context, antennas need to be properly analyzed for two reasons: On the one hand, multiband antennas will be progressively installed on aircraft and, therefore, the achievable performance at the L5/E5a band will be evaluated and properly described in the Minimum Operational Performance Specifications (MOPS). On the other hand, the impact that the antenna has had on the final navigation solution has been more thoroughly investigated over the last few years. Contributions have been published, for instance, by Amielh et al. (2018), Caizzone et al. (2019a, 2019b), Harris et al. (2017), as well as Raghuvanshi and Van Graas (2015). Moreover, activities in this respect are being performed at the standardization level (RTCA/EUROCAE/ICAO), with new antenna MOPS for DFMC antennas specified in DO-373 (RTCA, 2018). This renewed interest is bringing a better understanding of the group delay role to light, as well as that of the dominant role of the antenna working as a spatial filter with respect to multipath.

In the framework of the Dual-Frequency Multipath Model for Aviation (DUFMAN) project financed by the European Commission that aims to develop multipath models for dual-frequency navigation for avionics, the previously described methodology has been used and further developed. The process being chain-built led to the capability of predicting pseudorange errors caused by the user antenna and airframe-induced multipath by means of a tight integration of electromagnetic measurements and simulations.

In the present work, the activity done in order to gain more insight into the physical rationale of the impact of the antenna on multipath results will be described. First, a method to characterize antennas and their performance with respect to multipath rejection will be discussed. Multipath suppression capability indicators will be defined, which are able to properly quantify the capability of an antenna to attenuate (or not) incoming multipath. Moreover, the process developed in-house to account for the airframe will be described and validated by means of comparison with data from flight measurements.

Furthermore, the simulation capabilities described before will be used to consistently analyze major multipath sources and investigate different scenarios, taking into consideration different antennas, different positions on the aircraft, and different airframes. In a later section, the same approach will be used to investigate multipath levels for platforms with different multipath environments (such as business aviation aircraft and large commercial aircraft having antennas installed further back on the fuselage) and will highlight differences with the results obtained for commercial aircraft.

Finally, the results will be bounded toward the creation of a multipath model, fitting the requirements of the DFMC MOPS. More work in this area is surely needed to address the new research questions arising, as better stated in the conclusion of the paper.

2 | ANTENNA CHARACTERIZATION

2.1 | Antenna Group Delay Characterization

The first step to characterize antenna-induced errors is to characterize the antenna itself (e.g., as in Van Dierendonck and Erlanson [2007]). As demonstrated by Appleget and Bartone (2019), Caizzone, et al. (2019a, 2019b), and Murphy et al. (2007), antennas' intrinsic errors on GNSS pseudorange errors are caused by group delay variations. A limit on the allowable variations is also included in DO-373 (RTCA, 2018), the aviation dual-frequency MOPS document on antenna

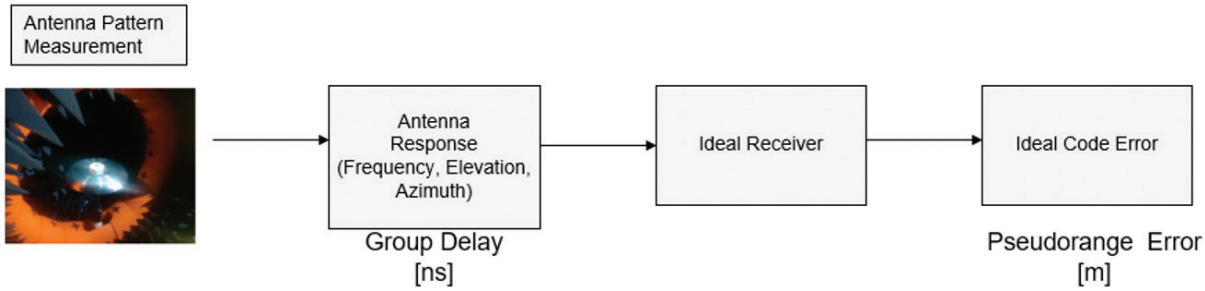

FIGURE 1 Functional flow diagram of procedure to characterize the antenna-induced error

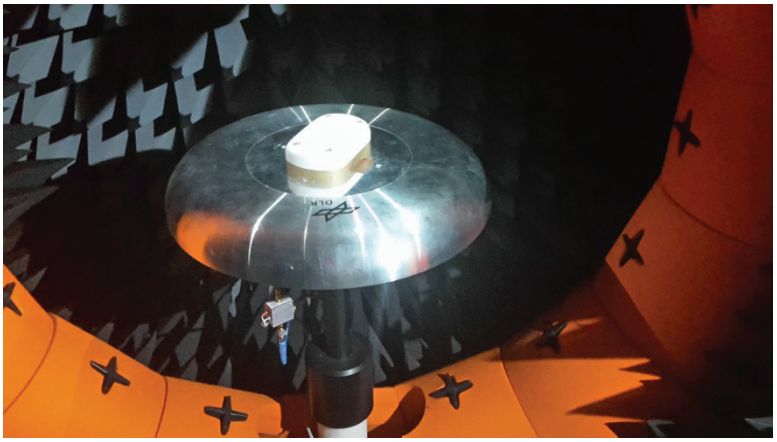

FIGURE 2 Commercial GNSS avionics antenna (Antenna B referred to in the text) mounted in the semi-anechoic chamber at DLR

performance. In order to characterize group delay variations and the related pseudorange error, we followed the procedure shown in Figure 1.

Two commercial antennas, hereafter referred to as Antenna A and Antenna B, are analyzed in depth in the rest of the paper. For the electromagnetic characterization, said antennas were installed on a rolled-edge ground plane and then measured in Microwave Vision Group's Starlab, a semi-anechoic chamber (Figure 1 and Figure 2) available on DLR premises.

The anechoic chamber measurement provides a transfer function of the antenna dependent on frequency, elevation, and azimuth angles. For the present work, frequency was sampled every 1 MHz (in a bandwidth of 24 MHz) and elevation/azimuth were sampled every 2 degrees. Group delay skyplots (proportional to the derivative of the phase over frequency) only consider one frequency: Exemplary results for the two antennas at one frequency (1176 MHz) are shown in Figure 3.

In order to assess the antenna-induced errors on each GNSS frequency band, it is important to properly weight the antenna transfer function with the GNSS signal spectrum. This was obtained by passing the antenna transfer function through an ideal receiver using the methodology shown in Vergara et al. (2016): Pseudorange errors (only due to the antenna and relative to the whole GNSS band) were obtained as outputs (as shown in Figure 4 and Figure 5).

For the present analysis, the configuration of the receiver was chosen according to the current draft material for standardization (i.e., 0.1 correlator chip spacing for L1/E1 and 1 chip for L5/E5a with a bandwidth of 24 MHz). The following signals were used depending on the frequency: BPSK(1) for L1 C/A, CBOC(6,1,1/11,-)

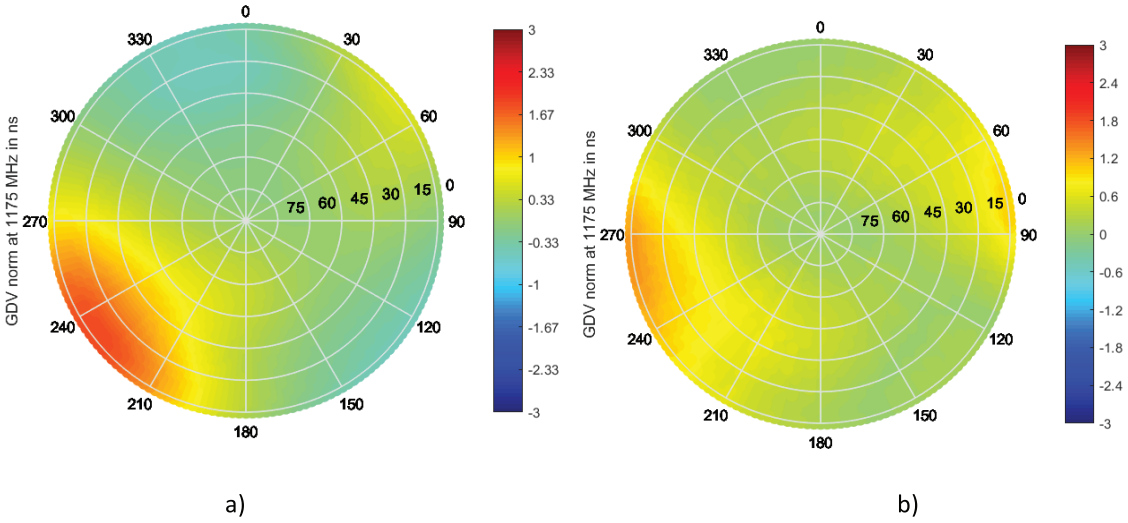

FIGURE 3 Group delay variations (normalized to zenith) in ns for (a) Antenna A and (b) Antenna B at 1176 MHz, as measured on the 0.4-m rolled-edge ground plane in Starlab chamber

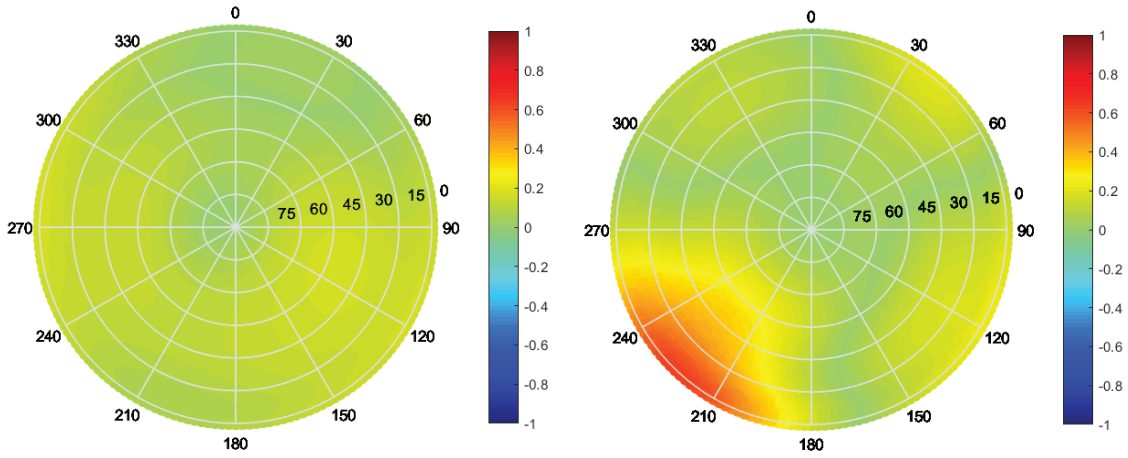

FIGURE 4 Pseudorange error (in m and normalized to zenith) obtained from the antenna measurement in Starlab and then processed through the ideal receiver for Antenna A at the L1 band (left) and at the L5 band (right)

for E1 OS, and BPSK(10) for L5 and E5a. Errors of up to more than 0.5 m were observed as they could clearly impact the quality of the positioning if not properly considered.

Differences in pseudorange error patterns shown in Figure 4 and Figure 5 are due to the intrinsic architecture of the antennas (because Antennas A and B are commercial products, their design is proprietary and not publicly available). An analysis of the behavior of group delay variations with respect to antenna architectures can, however, be found in Caizzone et al. (2019a, 2019b).

2.2 | Antenna Multipath Susceptibility Characterization

The former analysis showed a characterization of two commercial avionic antennas in terms of group delay variation and pseudorange error predictions. Such errors will add to the overall pseudorange error at the receiver if not properly

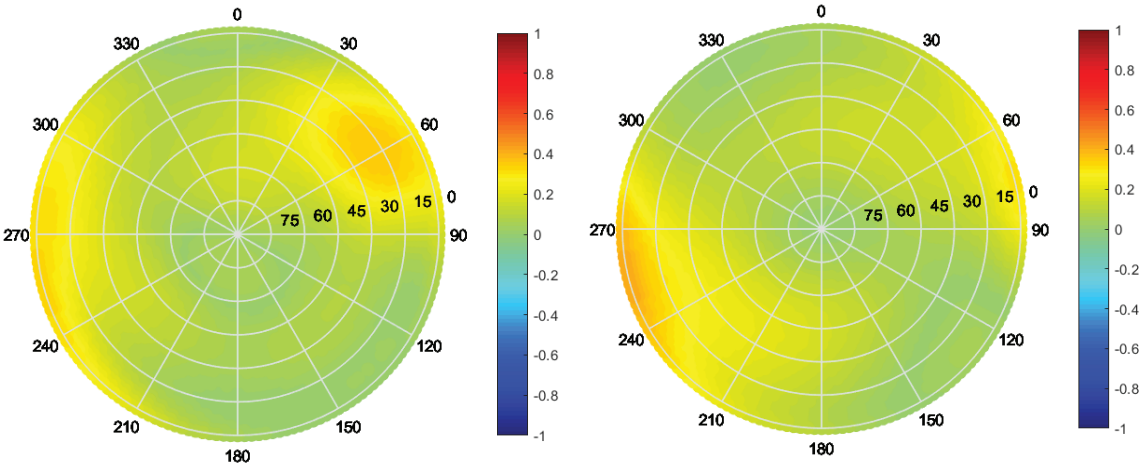

FIGURE 5 Pseudorange error (in m and normalized to zenith) obtained from the antenna measurement in Starlab and then processed through the ideal receiver for Antenna B at the L1 band (left) and at the L5 band (right)

considered (i.e., calibrated). However, apart from these error sources, due to their intrinsic properties, the antennas' impact on the overall error is also affected by the amount of multipath that the receiver is exposed to.

The antenna MOPS, however, only specify the antenna system, itself, and there is no direct connection to performance levels obtained on the receiver side yet. In particular, such connections appear very tricky for what concerns multipath performance.

In the currently valid single-frequency MOPS for satellite-based augmentation systems (RTCA DO-229), for instance, multipath was accounted for by a $\sigma_{multipath}$ term that was dependent on the elevation angle θ_i of the satellite, modeled as:

$$\sigma_{multipath}(i)[m] = 0.13 + 0.53e^{(-\theta i/10deg)}$$

Such a term has no clear correlation with antenna-specific requirements.

An improvement has been recently pursued in DFMC documents under development, with the *antenna* term being explicitly stated and combined with the multipath term in ED-259A, as also approved at the International Civil Aviation Organization (ICAO) level (Circiu et al., 2020b). More work in the area is surely needed to clearly associate antenna-related effects to the corresponding pseudorange error and its impact on, for example, protection levels.

The only requirement in the antenna MOPS that is currently linked with multipath errors (through a specification of the cross-polarization level of the antenna) is the axial ratio, which is defined as the ratio of the major axis to the minor axis of the polarization ellipse, having to be less than or equal to 3 dB in a region extending from boresight down to 40 degrees of elevation off boresight across all azimuth angles (RTCA DO-373, 2018). Such a parameter, though, useful to ensure good polarization purity of the antenna and, therefore, good reception of the desired signal, is, however, not fully representative of the multipath characteristics of antennas for two reasons.

First, the axial ratio only considers the goodness of the antenna in suppressing cross-polar radiation (i.e., multipath) coming from the *same angle* as the co-polar radiation (i.e., the satellite signal). In general, however, and even more in the aeronautic scenarios, such an assumption is not valid. In this case, multipath is most likely coming from directions other than that of the satellite signals (e.g., from low

elevations after reflections on tail or winglets). Moreover, the axial ratio is defined in the MOPS as only applicable for a portion of the hemisphere, namely for the most favorable one, around boresight. The behavior of the antenna in low elevations (where most multipath phenomena are expected) is left unspecified.

In previous work from the authors (Caizzone et al., 2018), more suitable parameters to describe the multipath-related characteristics of GNSS antennas have been identified. They have been called *multipath suppression capability indicators* (MPSIs) and have different formulations for different types of multipath (i.e., from the lower hemisphere, from the upper hemisphere, specular, diffuse).

In this work, a related parameter called the *multipath susceptibility ratio* (MPSR) is used as suitable for the aviation scenario (and more intuitive than the MPSI). The multipath susceptibility ratio is basically a worst-case undesired-to-desired ratio (i.e., a ratio between the maximum value of the Left-Hand Circularly Polarized (LHCP) gain in the upper hemisphere and the Right-Hand Circularly Polarized (RHCP) gain in the direction of the signal:

$$MPSR(\theta_s, \varphi_s) = \frac{\max\limits_{\forall\, \theta>0, \phi} Gain_{LHCP}(\theta, \phi)}{Gain_{RHCP}(\theta_s, \varphi_s)}$$

where $\theta \in (0°, 90°)$ and $\phi \in (0°, 360°)$ denote elevation and azimuth, respectively. In particular, the angles θ_s and ϕ_s denote the incident angles of the line-of-sight signal, for which the metric is evaluated. For the multipath, on the other hand, no a-priori knowledge about the angle of arrival is assumed, so that the worst case (i.e., the biggest value of the cross-polar gain $Gain_{LHCP}$ in the upper hemisphere) is taken into account.

It is worth noticing that the antenna, itself, cannot suppress any RHCP multipath due to the fact that the distinction between multipath and signal can only happen on the receiver side and not the antenna side. Therefore, the only possible multipath suppression on the antenna side for reflections in the upper hemisphere is related to the suppression of the LHCP gain.

An MPSR close to 0 dB means that the multipath is barely suppressed by the antenna (i.e., the multipath is as strong as the signal). On the other hand, an MPSR of about –20 dB means that the multipath will be attenuated by 20 dB with respect to the direct signal.

When evaluating the MPSR for all possible angles, a 3D map is obtained giving an indication of the capability of the antenna to suppress multipath amplitude, which is variable according to the angle. An example is given in Figure 6 and Figure 7 for the two commercially available antennas under consideration for the L1/E1 and L5/E5a bands.

2.3 | Antenna Installed Performance Characterization

From the previous discussion, it is clear that antennas act as spatial-polarimetric filters and such antenna characteristics strongly influence the amount of multipath passed to the receiver. In order to investigate and demonstrate its use in the aviation context, the process described in Figure 1 was extended to be capable of integrating the electromagnetic measurement of real commercial-off-the-shelf (COTS) avionic antennas with a simulation of said antenna on a given platform (in our case, on a CAD model of an airplane; in this case, Airbus A320). Such a process enables us to obtain the *installed antenna response* (dependent on frequency, elevation, and azimuth) containing the contributions of both actual antennas per

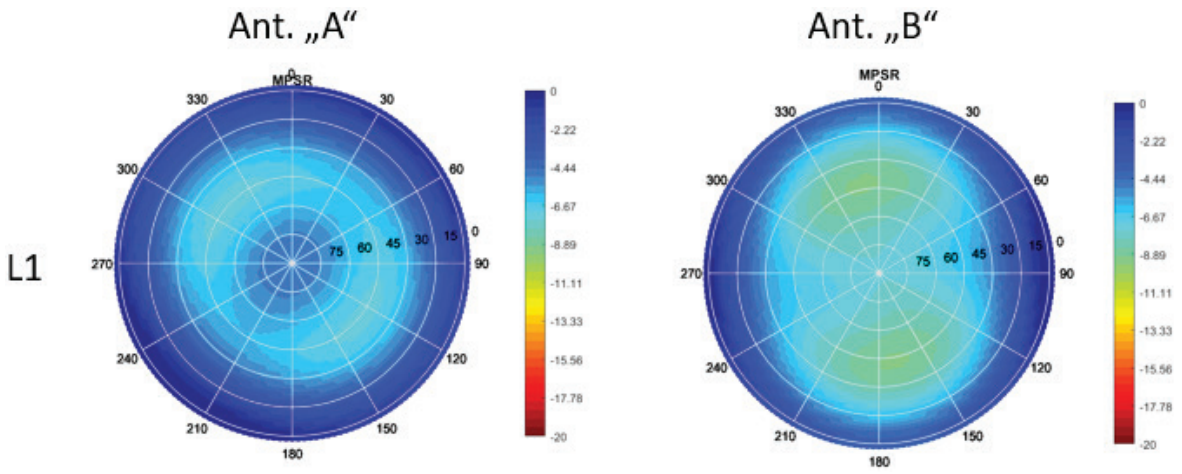

FIGURE 6 MPSR (in dB) for Antennas A and B (on the left and on the right, respectively) at the L1 band

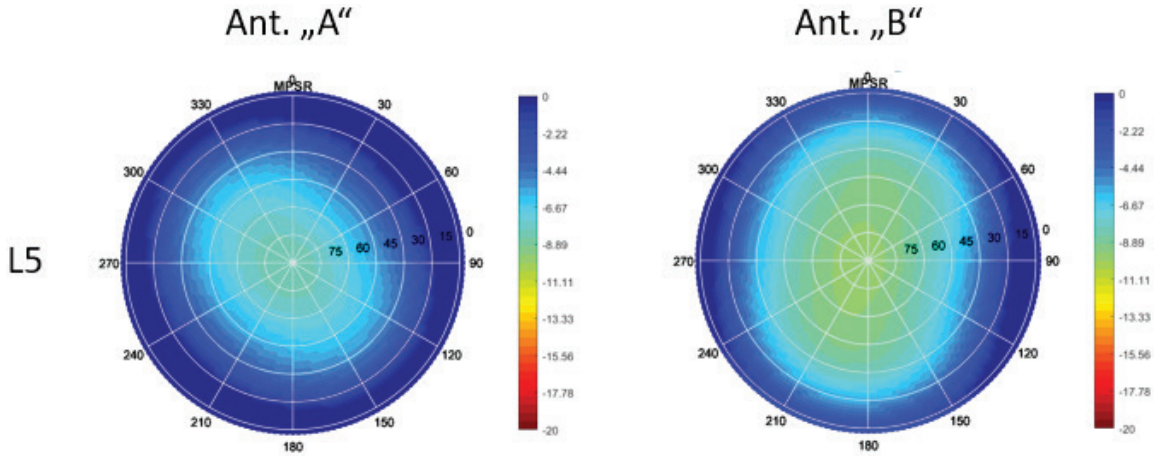

FIGURE 7 MPSR (in dB) for Antennas A and B (on the left and right, respectively) at the L5 band

se and that of the interaction with the airplane (i.e., due to the multipath of the airplane). By passing this response through an ideal software receiver, it was possible to estimate the pseudorange error produced by the specific installation of that antenna on that position of that airplane (Figure 8).

It is worth highlighting here that in order to analyze the impact of the antenna on the multipath contribution, there is a need to de-embed the antenna-only errors (as calculated in the former section) from the overall results by a calibration step, as reported in Circiu et al. (2020c).

For example, the multipath (and noise) contribution is shown in Figure 9 over elevation before and after calibration. The calibration step basically removes the antenna group delay variation error from each raw pseudorange measurement according to the respective angle of arrival of the satellite (corresponding to a specific antenna group delay variation error) before statistical processing is started.

In this way, the antenna impact due to multipath suppression capability can still be considered while its intrinsic error due to group delay variations is not. This separation allows us to perform an analysis of the multipath contribution for different antennas.

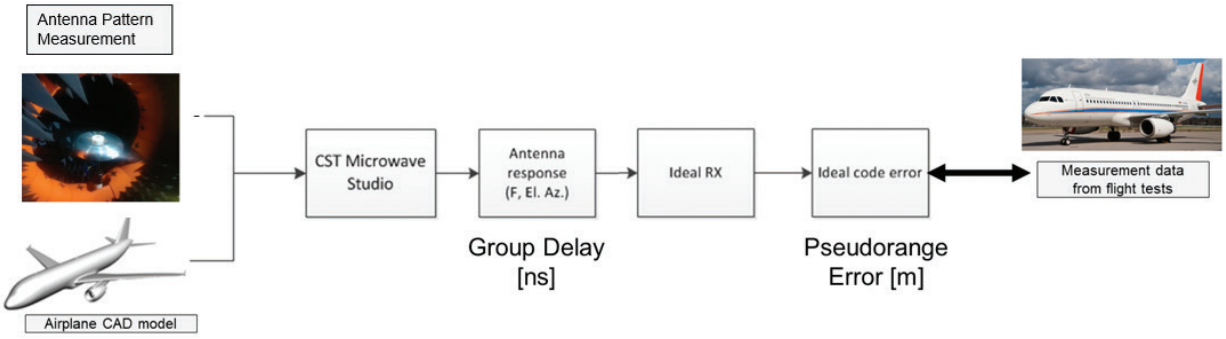

FIGURE 8 Functional flow diagram of the process to obtain pseudorange errors starting from electromagnetic measurement of the antenna

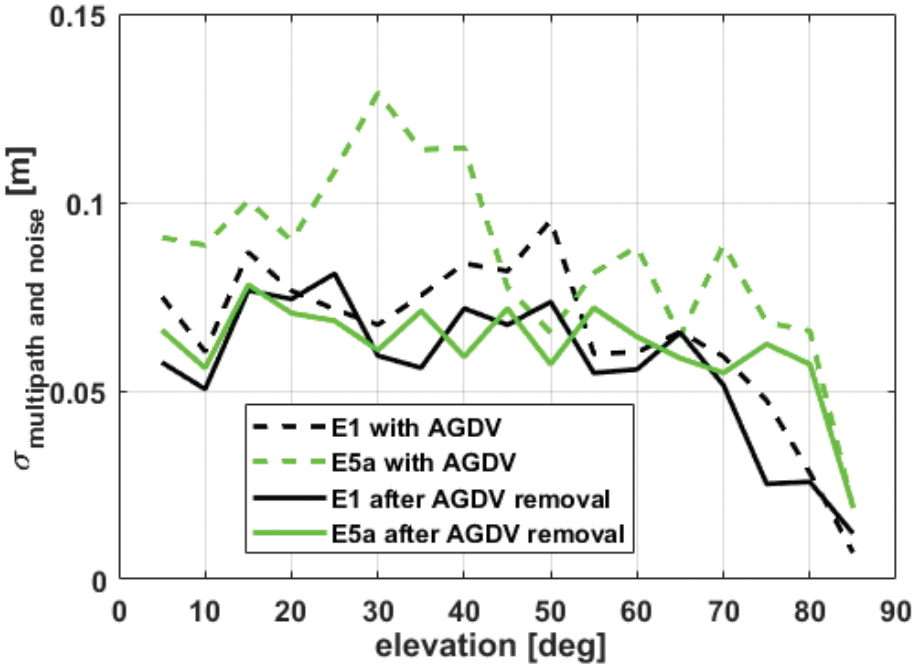

FIGURE 9 Multipath versus elevation for E1 and E5a with antenna errors and after antenna error removal (Note: AGDV refers to antenna group delay variations)

The result of the formerly described process is found in a 3D map of the predicted multipath (at each GNSS band) for that specific installation (expressed as skyplot or as 2D Map, see Figure 10). It was, then, possible to compare it with the data obtained from flight test measurements and processed to isolate the multipath-only component (i.e., by using the dual-frequency dual-constellation code-minus-carrier [CMC] method [Circiu et al., 2020c]).

An exemplary comparison for one satellite (PRN 9) between the flight data ("measurement") and the data from the installed performance simulation ("simulations") is shown in Figure 11. Simulations very closely follow the shape of the measured multipath.

The absolute values differ slightly as the measurements were affected by further errors (such as receiver imperfections, atmospheric effects, etc.) that were not considered in the simulation. Moreover, the simulated data were obtained

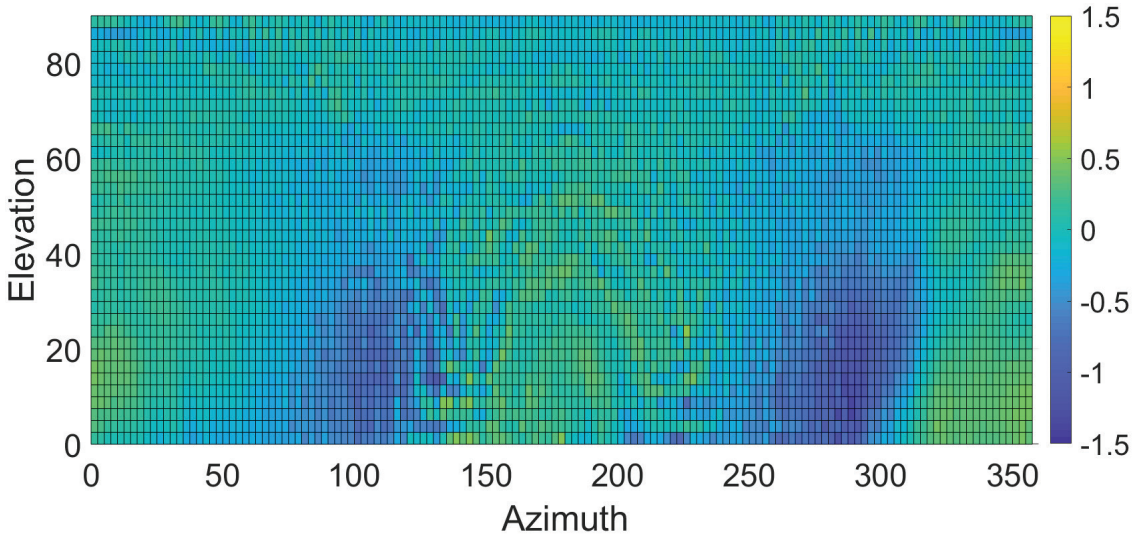

FIGURE 10 3D map of the predicted multipath error (normalized to zenith and with antenna-intrinsic error calibrated out) of Antenna A at the L1/E1 band

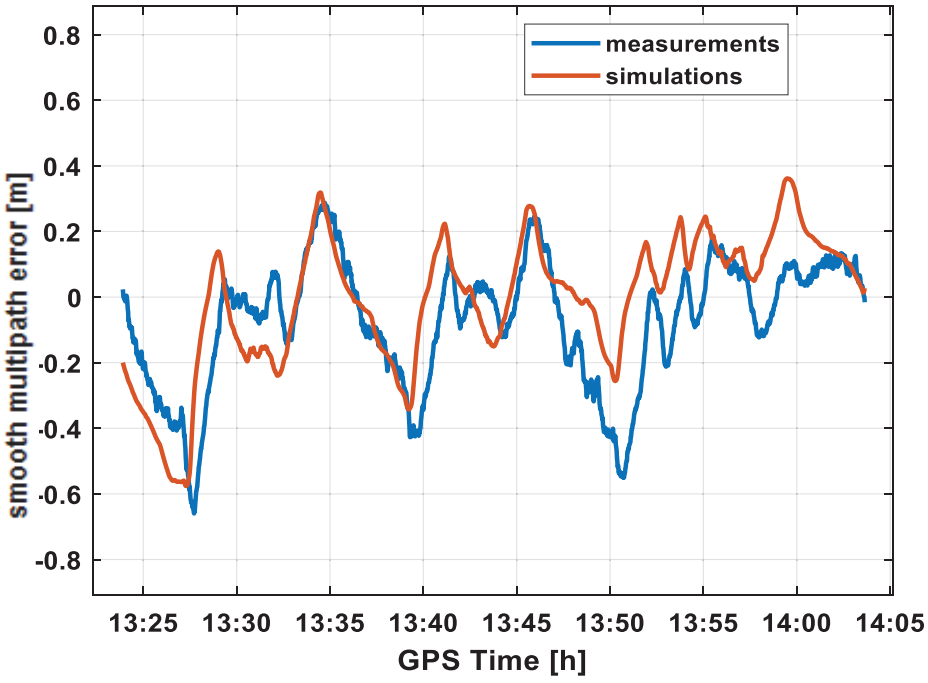

FIGURE 11 Comparison of the 100s smooth multipath error obtained by processing GNSS data from flight tests in code-minus-carrier technique and synthetic data obtained by electromagnetic simulation of the installed performance of Antenna A on A320 aircraft

strongly simplifying the scenario, considering a simplified full-metal aircraft and not changing its setup during flight (i.e., not considering wing flex and further effects).

An extensive use of electromagnetic simulation will be presented in the next section to gain further insight into the physics of multipath on aircraft structures in avionic applications.

3 | EXPLOITING SIMULATION CAPABILITIES TO OBTAIN INSTALLED PERFORMANCE

The simulation capabilities established and described in the former section can be exploited to gain insight into the phenomena underlying the multipath results on aircraft, as well as providing the means to perform an analysis of the expected multipath on different platforms. This has the strong advantage, on one hand, to make a step-by-step analysis possible (for instance, by analyzing the effects of different parts of the airplane) and, on the other hand, it allows for the analysis of multipath in scenarios for which no flight data is yet available (e.g., for new aircraft or for different antennas that are not certified for flight). It is worth mentioning that the simulations consider a realistic but simplified model of the aircraft and that the airframe is, for simplicity, considered here to be fully metallic.

3.1 | Impact of Different Parts of the Airframe

An Airbus A321NEO was taken as a reference with an antenna placed at the standard GPS Position 2 (i.e., roughly above the entrance door toward the front of the plane and on the top centerline). The airplane was simulated considering progressively more and more components of the structure so a better understanding of the objects causing reflections becomes possible (see Figure 12). In particular,

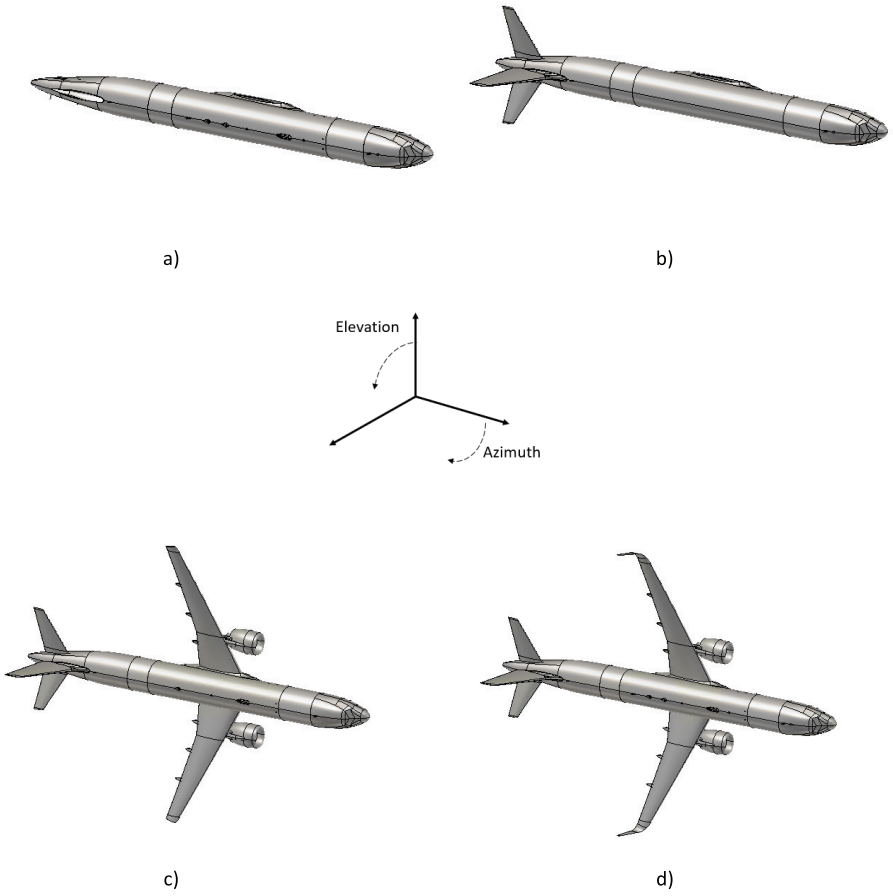

FIGURE 12 Different parts of the A321NEO aircraft considered in the installed performance analysis to identify the sources of multipath: a) fuselage only; b) fuselage and tail; c) fuselage, tail, and wings (without winglets); and d) full aircraft

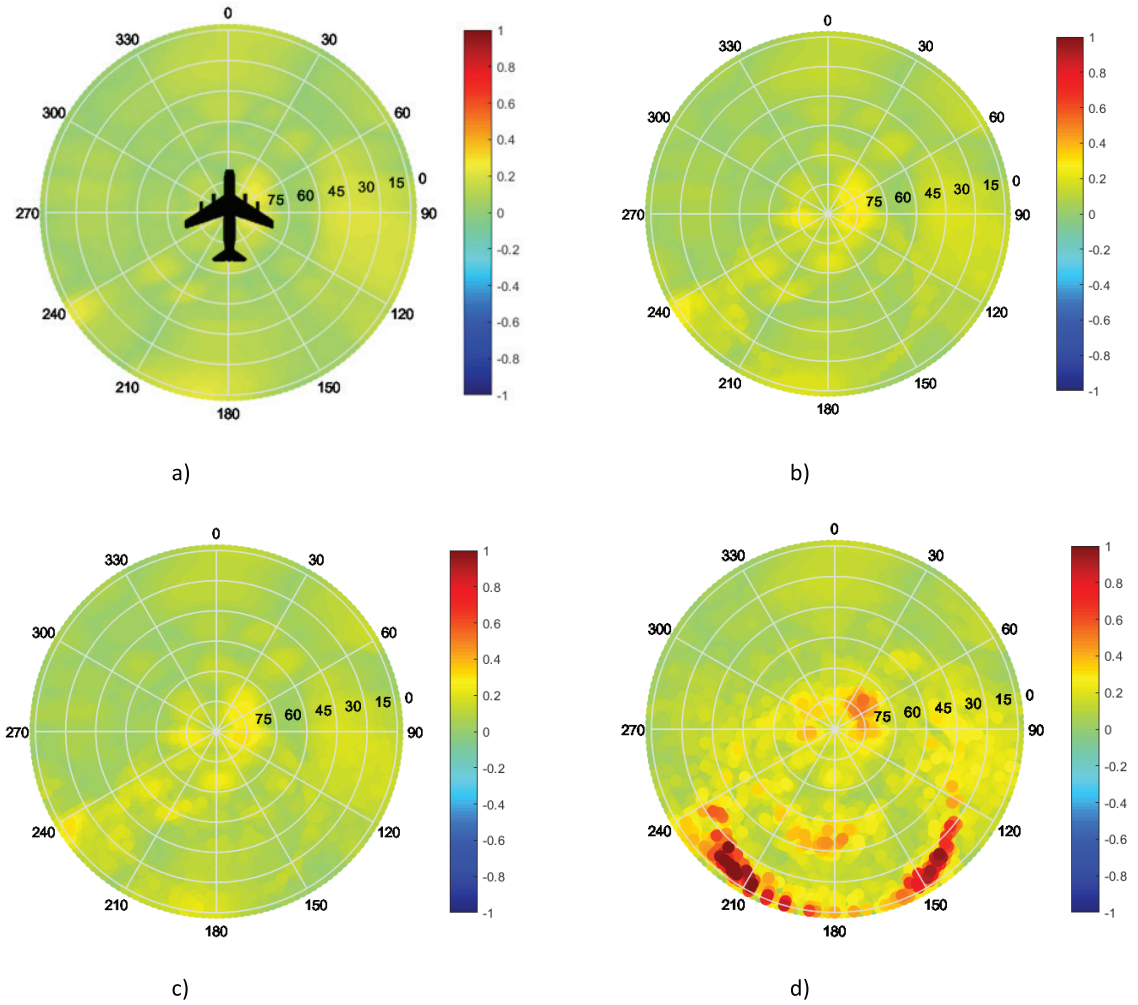

FIGURE 13 Skyplot of multipath error, calibrated and normalized to zenith, for Antenna A on A321NEO, Position 2, at the L1 band considering: a) fuselage only; b) fuselage and tail; c) fuselage, tail, and wings (no winglets); and d) full aircraft

the simulations shown here are comprised of the following structural parts of the aircraft:

- fuselage only
- fuselage and tail
- fuselage, tail, and wings (without winglets)
- full aircraft

The airframe multipath error prediction results shown are both in terms of skyplots (Figure 13) as well as versus elevation angle (with respect to the aircraft body frame) with a plot of the average value with error bars to show the maximum and minimum values found over azimuth at the given elevation bin (Figure 14). The analysis was performed with Antenna A. The difference obtained when using Antenna B will be shown later. The orientation of antenna with respect to aircraft is shown in Figure 13a and will be valid for all plots.

Please note that, in this calculation, no smoothing is applied (differently from the processing performed during real flights, where 100s smoothing is applied to

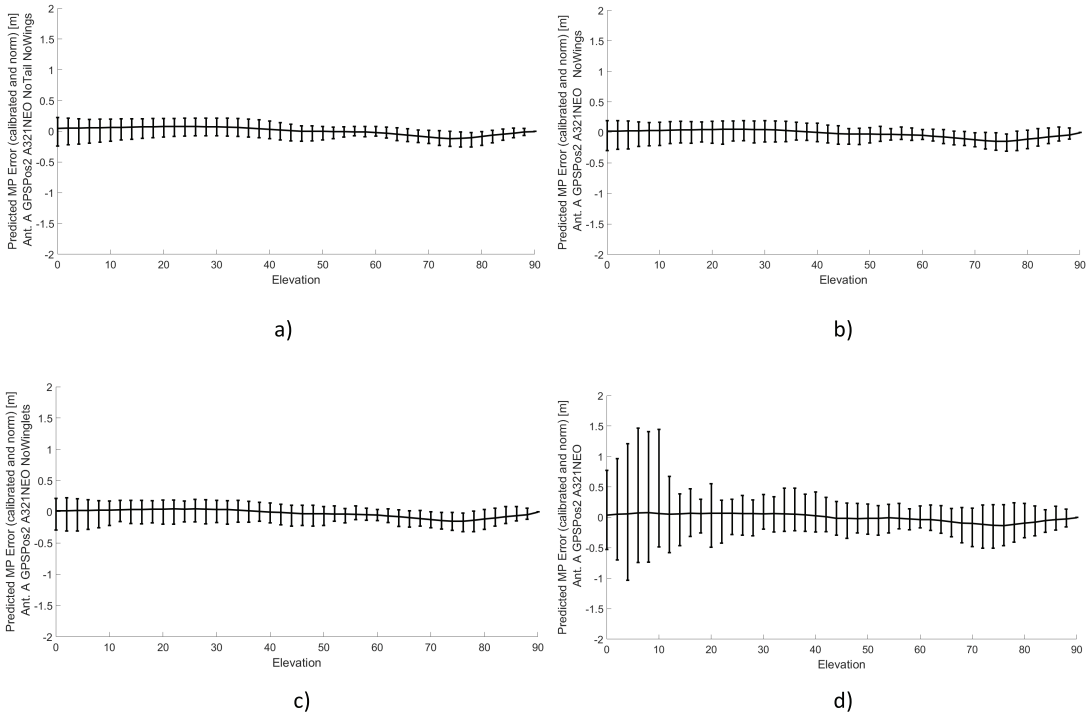

FIGURE 14 Multipath on L1 band vs elevation for Antenna A on A321NEO, Position 2, considering: a) fuselage only; b) fuselage and tail; c) fuselage, tail, and wings (no winglets); and d) full aircraft

reduce multipath effects). Results shown in this section are representative of raw multipath.

Figure 13 and Figure 14 clearly show the impact of the tail on the aircraft multipath error at high elevations, as well as the even more relevant effect of wings/winglets for low elevations. For the A321NEO example, the winglets appear to have the most impact, as they are more clearly visible from the antenna standpoint. Other airplanes having strongly slanted wing configurations will also experience a similar impact due to the wing tips. Such structural parts appear, therefore, to be the dominant sources of multipath.

3.2 | Impact of Different Antennas

In order to investigate the impact of different antennas, Antenna B was simulated on the same aircraft in the same position as Antenna A. Results are shown in Figure 15 and Figure 16 for A321NEO at both the L1 and L5 bands. Bars in the plots express the minimum and maximum values obtained in the corresponding elevation bin.

Moreover, simulations were also performed with Airbus A330[1], placing the antenna again in primary position GPS Position 2. Results are shown in Figure 17 and Figure 18. Though the shape of the curve is roughly similar among the two antennas for the same aircraft (due to similar multipath environment determined by the installation geometry), the amplitudes differ. In particular, Antenna A appears to produce slightly larger errors on the L1/E1 frequency band than Antenna B. The

[1]The choice of aircraft is tightly aligned to the type of aircraft flown in the measurement campaign during the DUFMAN project for which a CAD model was provided by project partner Airbus

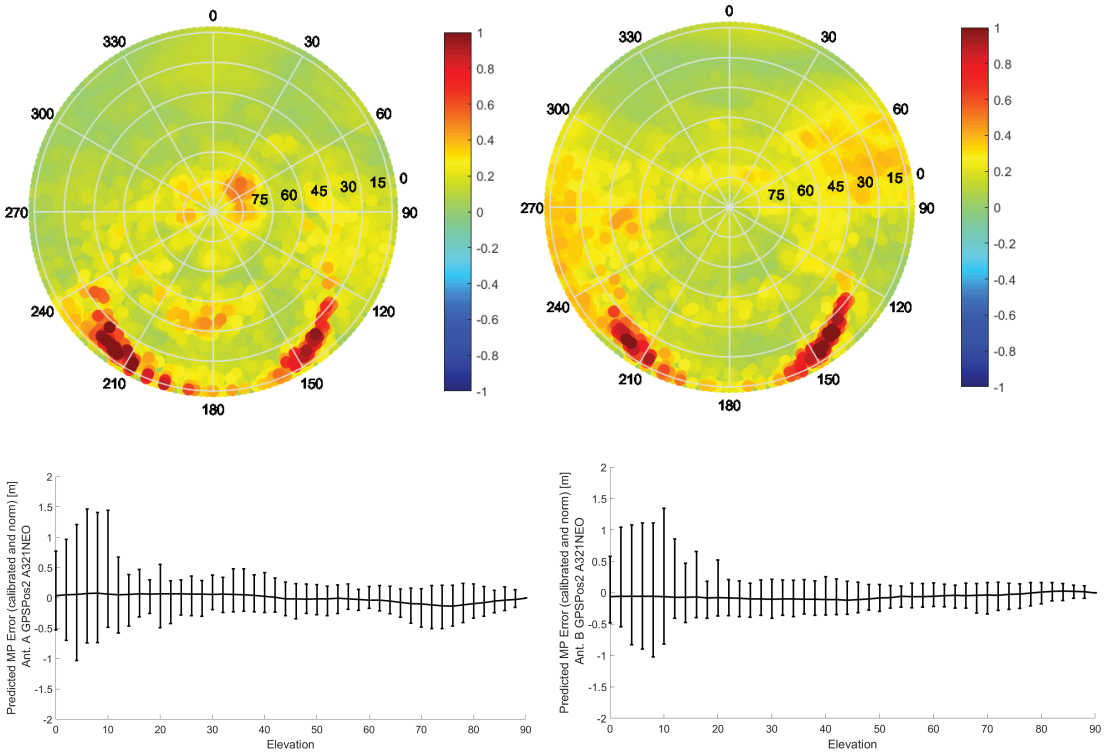

FIGURE 15 Predicted multipath error (in m) as a skyplot (top) or versus elevation (bottom) at the L1 band for Antenna A (left) and Antenna B (right), installed in the primary position GPS Position 2 on the A321 NEO aircraft

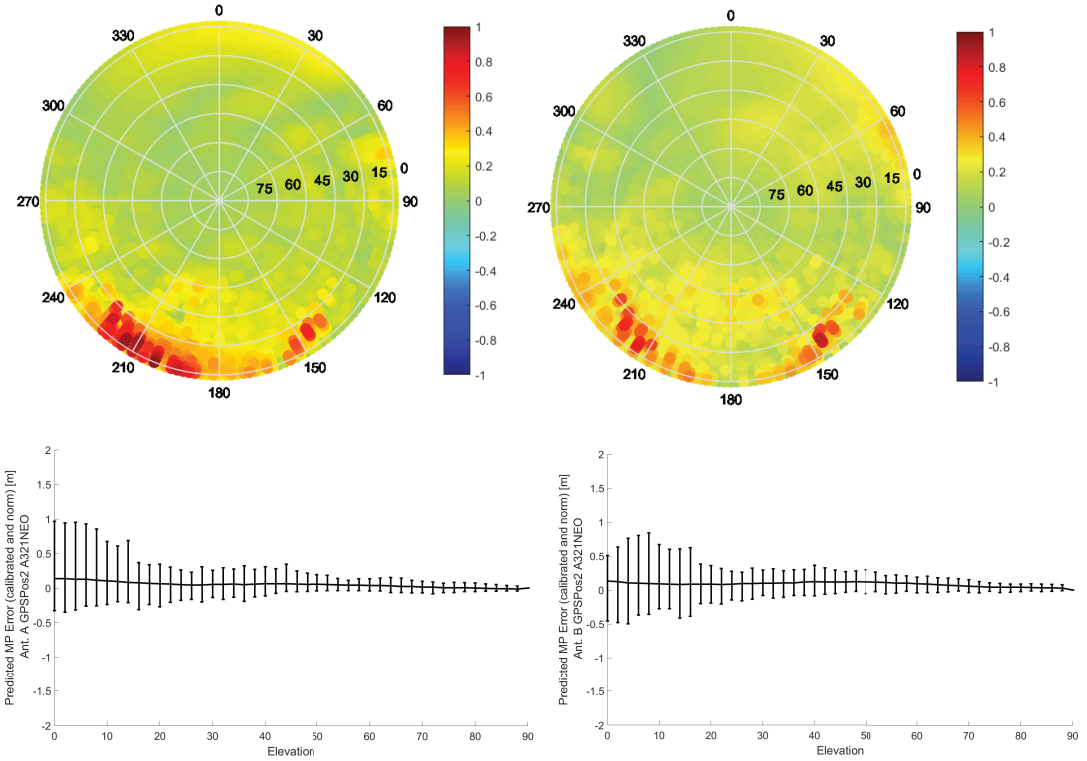

FIGURE 16 Predicted multipath error (in m) as a skyplot (top) or versus elevation (bottom) at the L5 band for Antenna A (left) and Antenna B (right), installed in the primary position GPS Position 2 on the A321 NEO aircraft

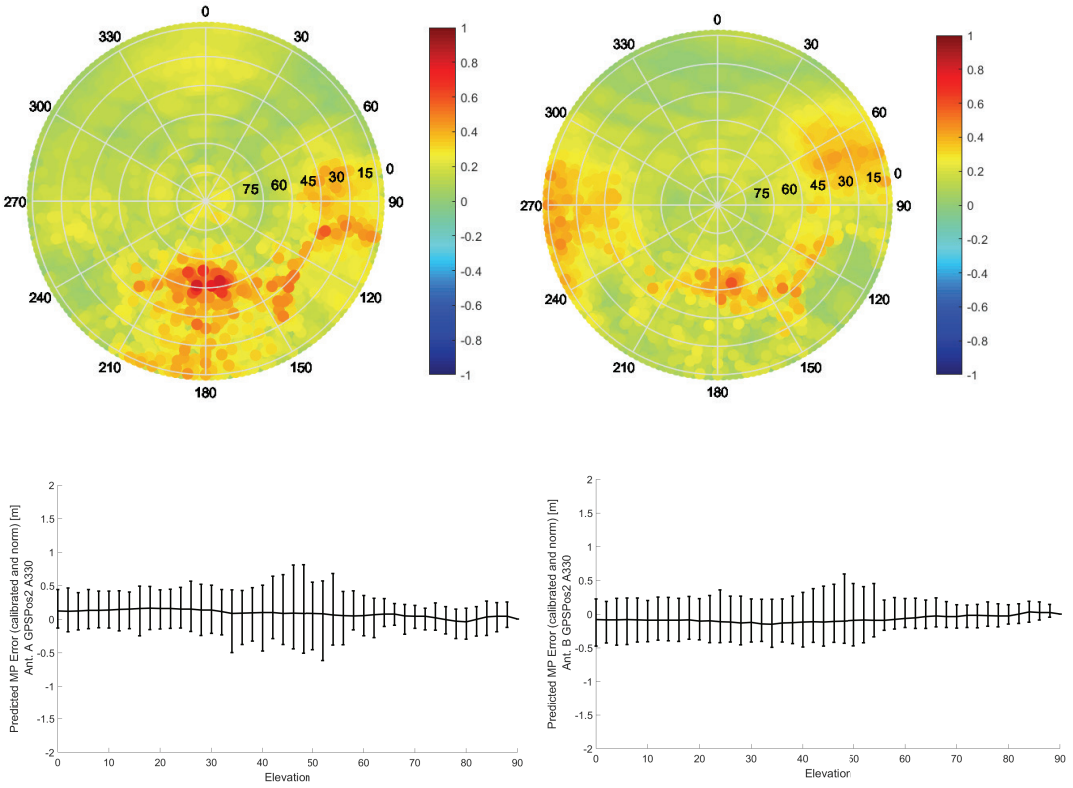

FIGURE 17 Predicted multipath error (in m) as a skyplot (top) or versus elevation (bottom) at the L1 band for Antenna A (left) and Antenna B (right), installed in the primary position GPS Position 2 on the A330 aircraft

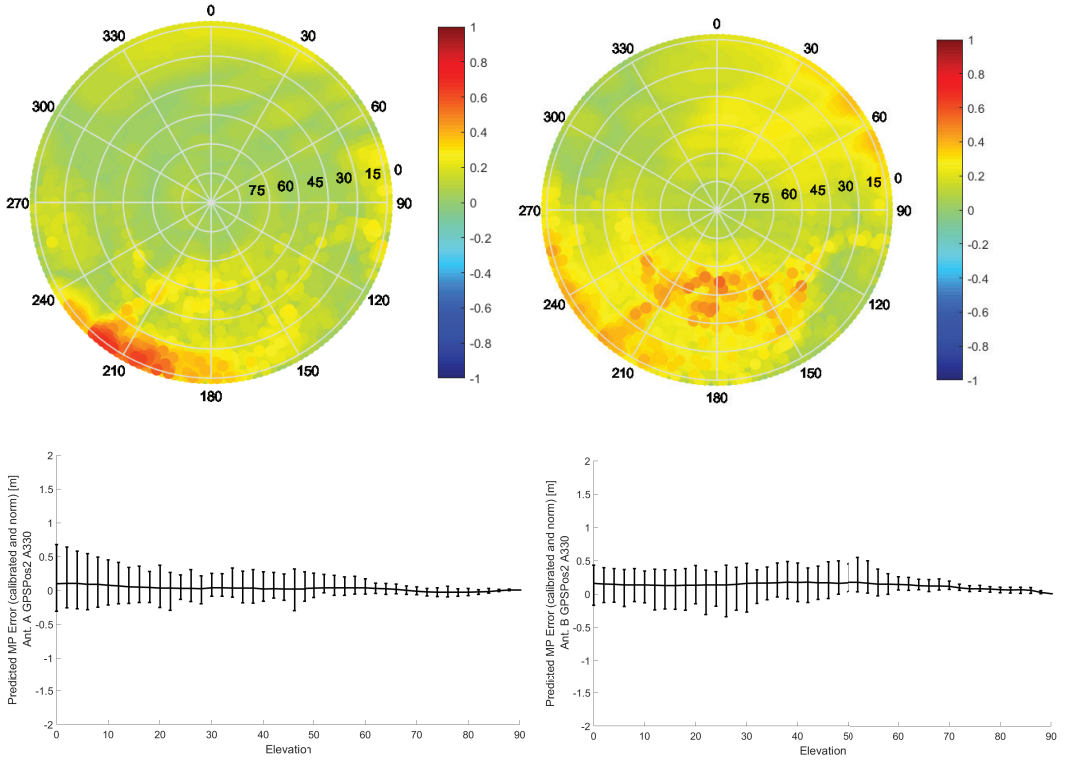

FIGURE 18 Predicted multipath error on L5 band (in m) as a skyplot (top) or versus elevation (bottom) for Antenna A (left) and Antenna B (right), installed in the primary position GPS Position 2 on the A330 aircraft

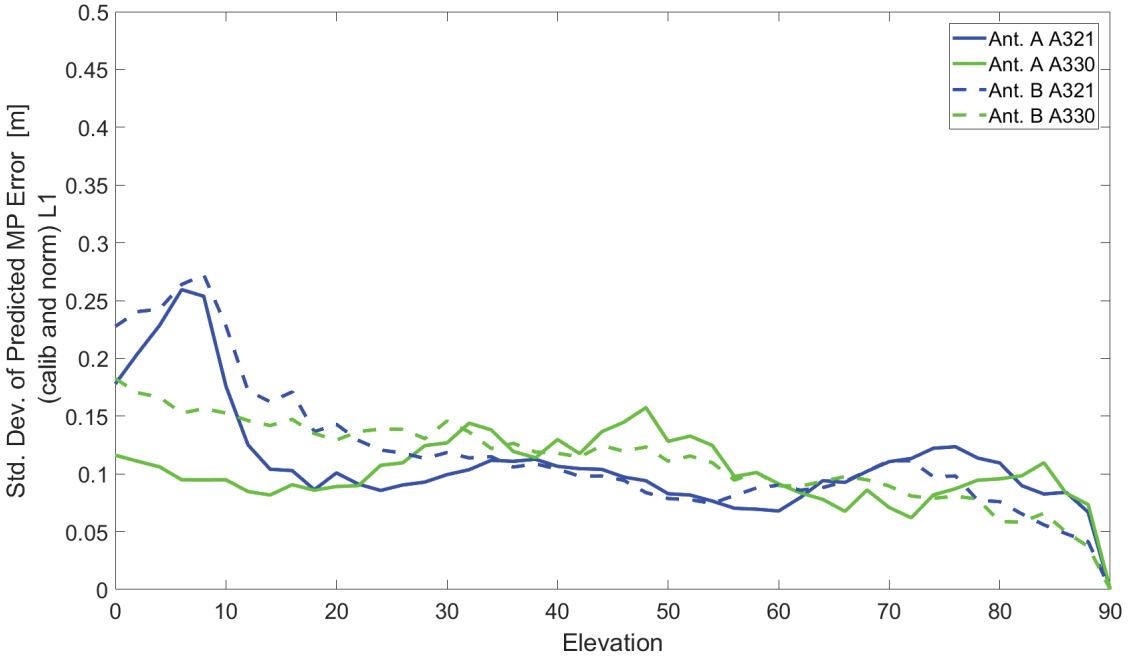

FIGURE 19 Standard deviation of the predicted multipath error (in m, calibrated for antenna-intrinsic pseudorange error and normalized to zenith) at the L1 band for Antennas A and B from the installed performance simulations on A321NEO and A330 aircraft

difference between the two antennas for the L5/E5a band is larger, especially at low elevation angles.

An explanation for this phenomenon can be found in the multipath suppression capability of the two antennas introduced in previous section. Antenna A's MPSI values were worse than that of Antenna B and this difference is even stronger at the L5 band for low elevations (Figure 6). Even if the signal on the L5/E5a band had better multipath rejection capabilities on long delay multipath, for short range multipath below 30 m (dominant in this scenario), the expected multipath code error on the L1/E1 and L5/E5a bands is similar. However, it can be also noticed that, though using two totally different antennas, the amount of multipath error did not differ substantially for both bands.

Figure 19 and Figure 20 show the standard deviation of the predicted multipath to be comparable with metrics used in MOPS[2]. It can be observed that the difference among the results obtained for the two antennas is not really substantial (on the order of a few cms). This can be explained by the fact that the considered installation point of the antenna (primary position GPS Position 2) is, indeed, a point where impinging multipath levels are low. Therefore, differences in the filtering capability of the antenna will not have too much of an impact. In order to analyze whether further installation points appear to be more challenging from a multipath point of view, further simulations are performed in the next section.

3.3 | Impact of Different Antenna Locations

In order to investigate the impact of different installation points, we considered the A350 aircraft, identifying two different locations: The primary position (GPS

[2]Please note that the predicted multipath error calculated here can be compared to raw multipath error as calculated from GNSS measurements through CMC techniques (and hence include no smoothing)

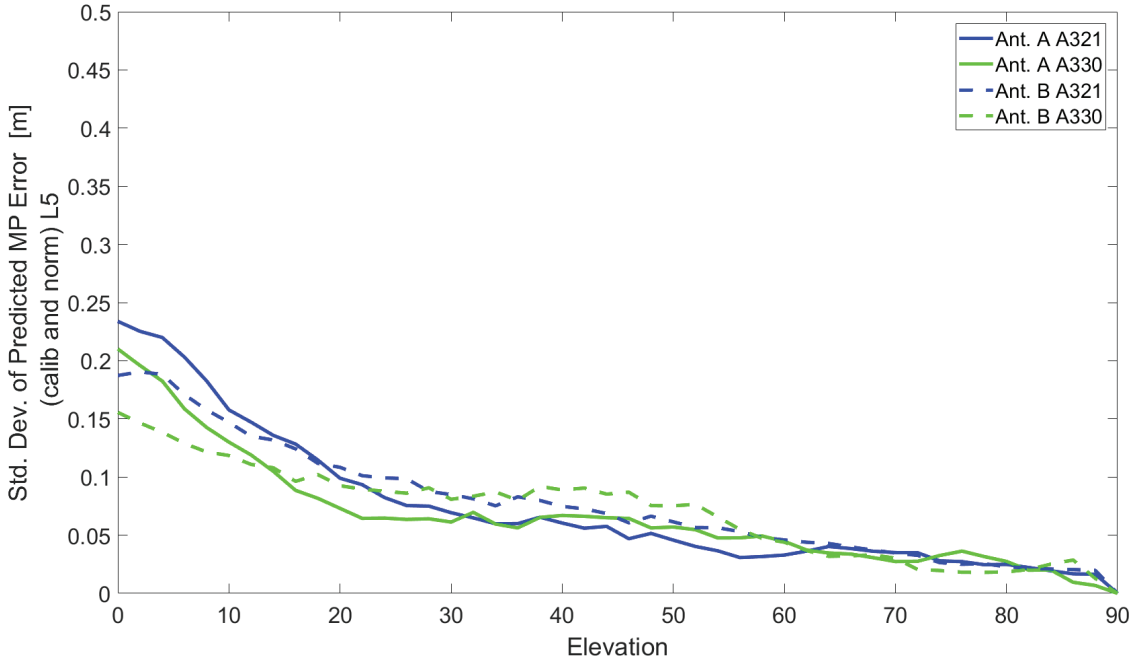

FIGURE 20 Standard deviation of the predicted multipath error (in m, calibrated for antenna-intrinsic pseudorange error and normalized to zenith) at the L5 band for Antennas A and B from the installed performance simulations on A321NEO and A330 aircraft

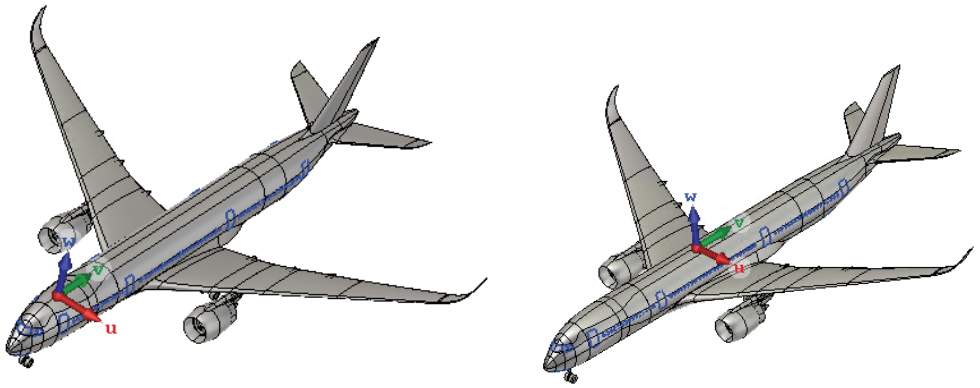

FIGURE 21 A350 CAD model with indication of the position of the GPS Position 2 (left) and the ADF position (right)

Position 2) as well as the Automatic Direction Finder (ADF) position (Figure 21). The ADF position resembles the installation point (in terms of ratio of the antenna position to the fuselage) on aircraft from other manufacturers and will, therefore, provide valuable information on the multipath to be expected in such cases.

In this case, two effects can be observed: On the one hand, the ADF position (due to its closer vicinity to the wings and tail and the even better visibility of the tail from antenna position) appears to be much more affected by multipath than Position 2 (i.e., cannot be considered a low-multipath position; see Figures 22 through 25). On the other hand, it is also evident how Antenna B, in the case where the environment is rich in multipath, manages to suppress the amount of multipath much better than Antenna A thanks to its better MPSR (see Figure 6 and Figure 7).

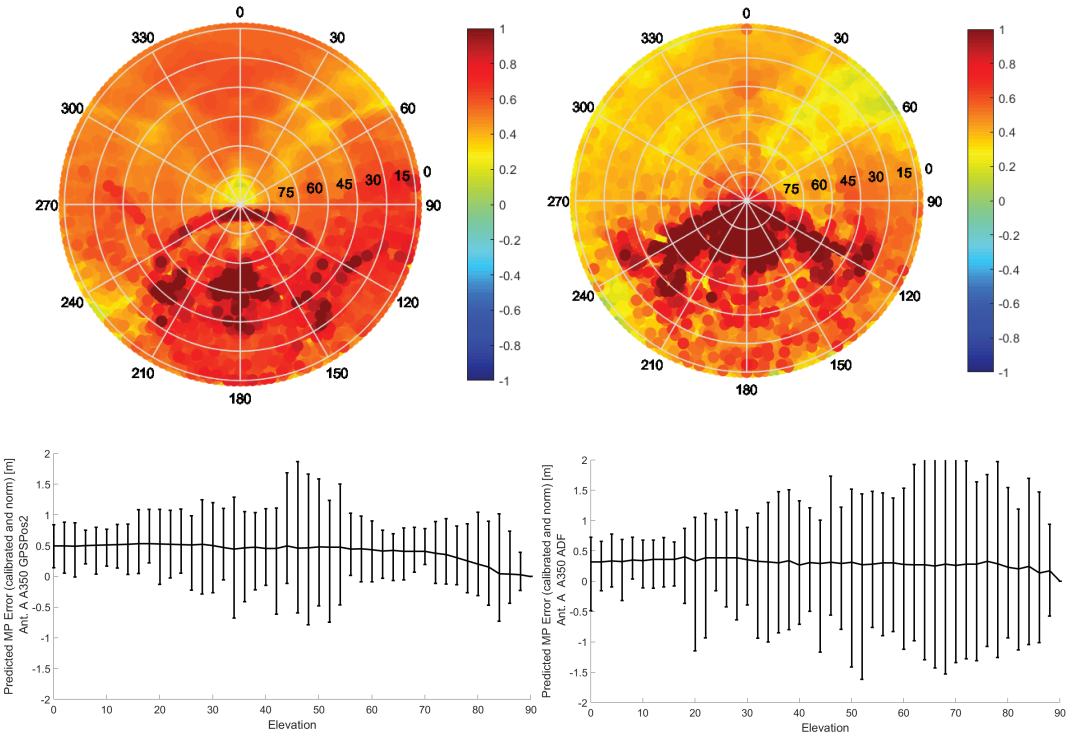

FIGURE 22 Predicted multipath error (in m) as a skyplot (top) or versus elevation (bottom) at the L1 band for Antenna A, installed in the primary position GPS Position 2 (left) and in the ADF position (right) on an A350 aircraft

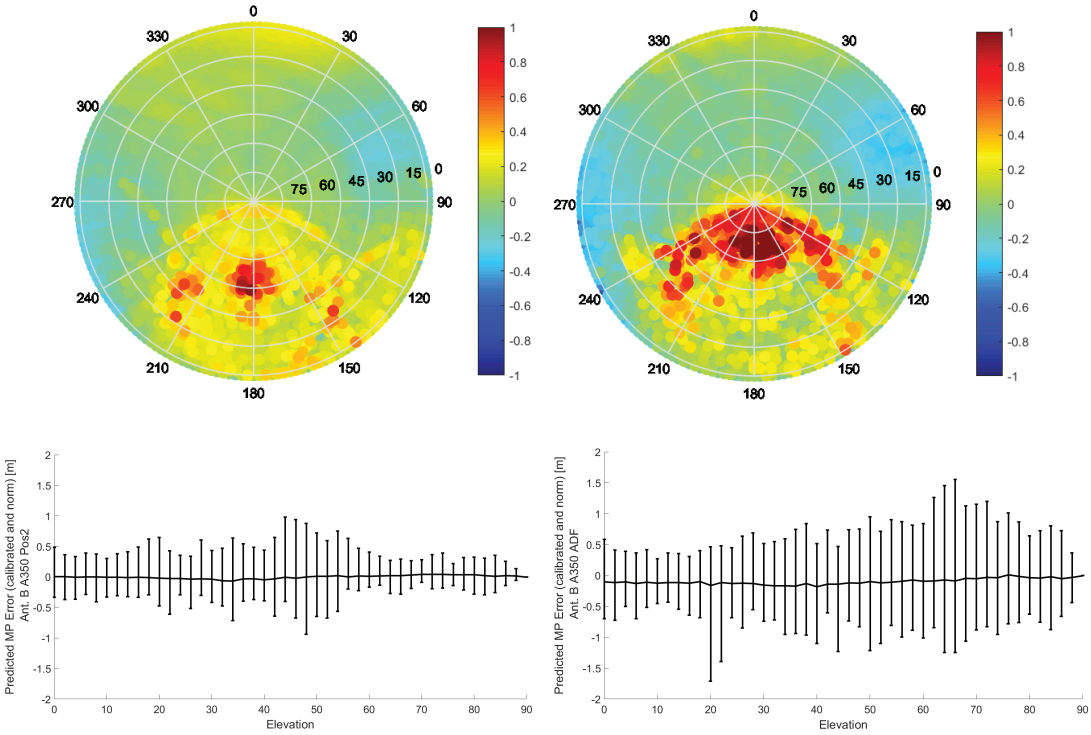

FIGURE 23 Predicted multipath error (in m) as a skyplot (top) or versus elevation (bottom) at the L1 band for Antenna B, installed in the primary position GPS Position 2 (left) and in the ADF position (right) on an A350 aircraft

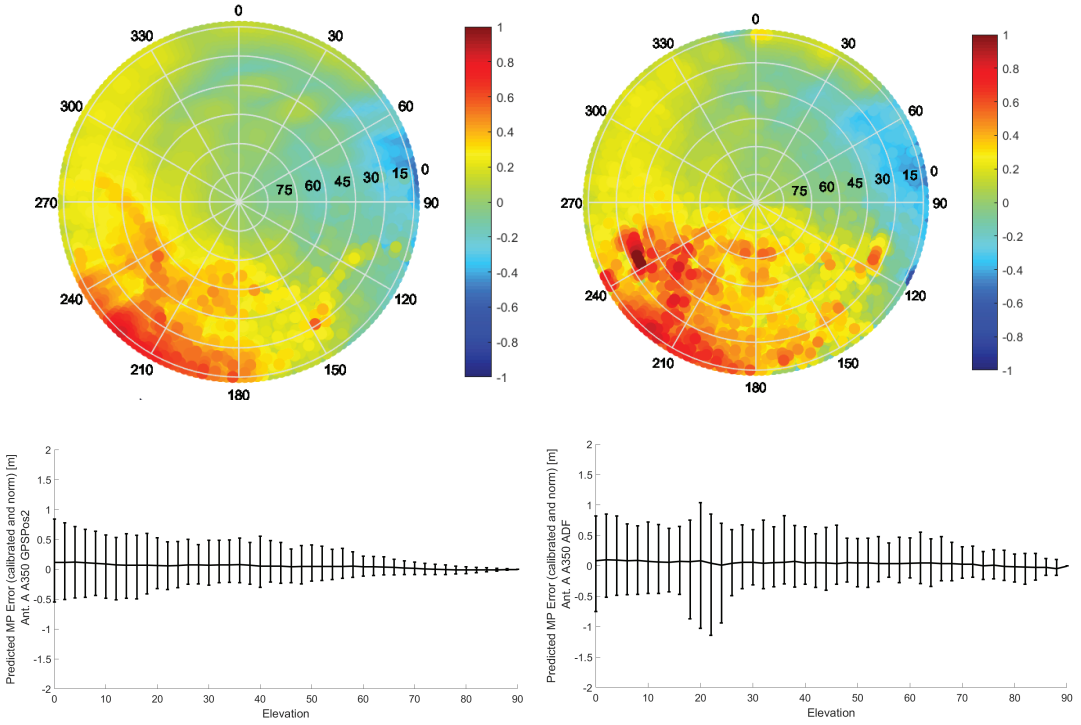

FIGURE 24 Predicted multipath error (in m) as a skyplot (top) or versus elevation (bottom) at the L5 band for Antenna A, installed in the primary position GPS Position 2 (left) and in the ADF position (right) on an A350 aircraft

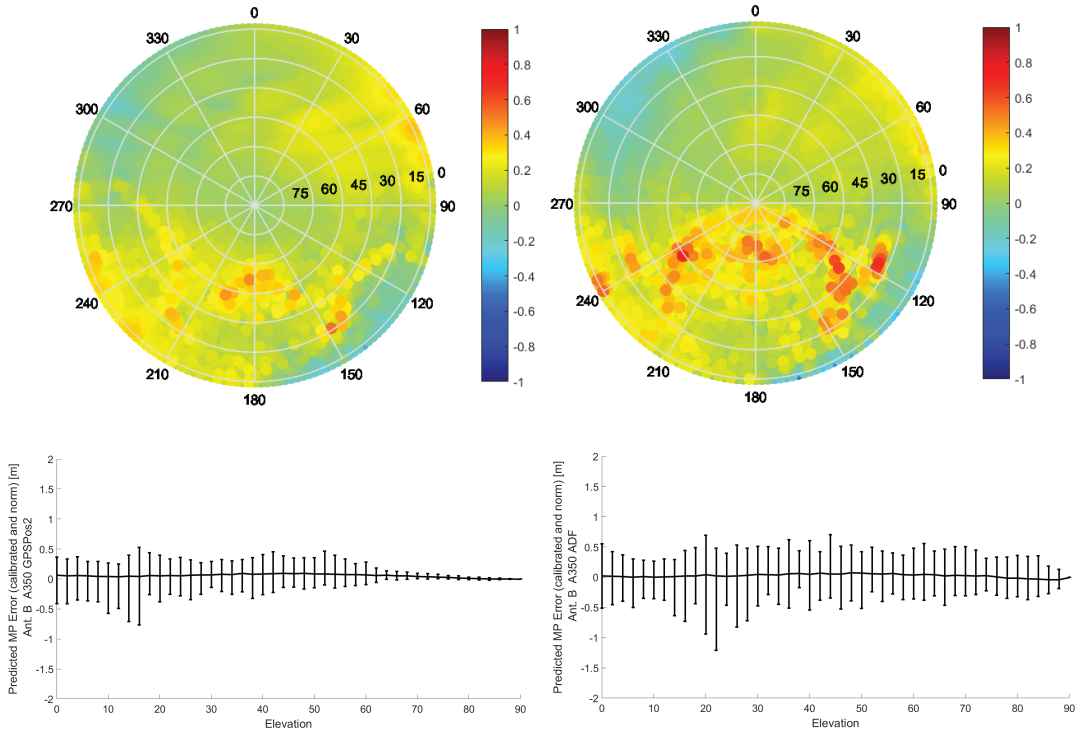

FIGURE 25 Predicted multipath error (in m) as a skyplot (top) or versus elevation (bottom) at the L5 band for Antenna B, installed in the primary position GPS Position 2 (left) and in the ADF position (right) on an A350 aircraft

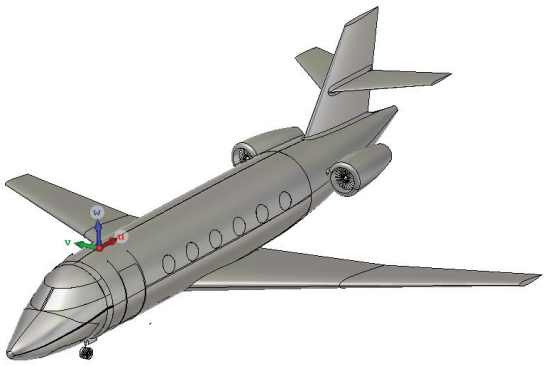

FIGURE 26 CAD model of a Falcon 200, with indication (center of coordinate system) of the antenna position (Position 1)

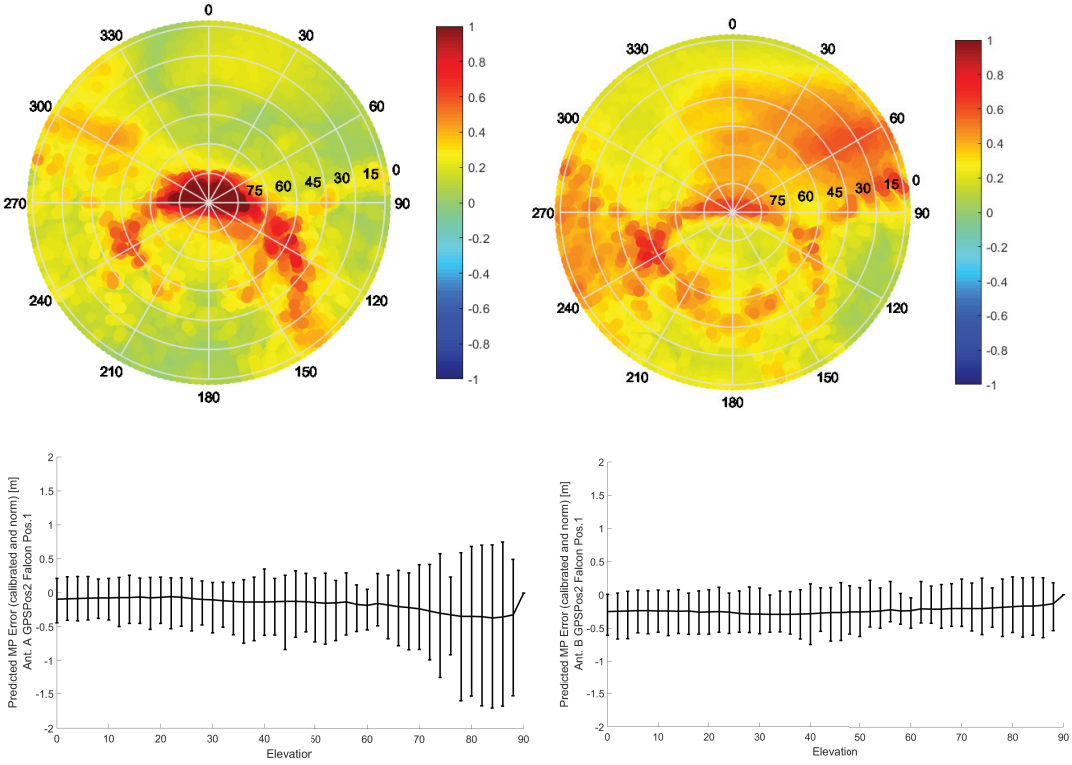

FIGURE 27 Predicted multipath error (in m) as a skyplot (top) or versus elevation (bottom) at the L1 band for Antenna A (left) and Antenna B (right), installed in the GPS Position 1 on a Falcon 200 aircraft

A further example of installation in a less multipath-benign environment can be obtained when considering a small business aviation aircraft like a Falcon 200 (seen in Figure 26). In this case, the distance between the antenna and relevant mechanical structures (T-tail, propellers, wings) is shorter and the visibility of those structures from the antenna is high.

Indeed, as Figure 27 and Figure 28 show, a strong multipath can be seen, as well as a relevant suppression observed when using Antenna B. The strong multipath for satellites coming from high elevations could be related to reflections from the tail as shown in Figure 29. The effect is more visible on the L1/E1 band

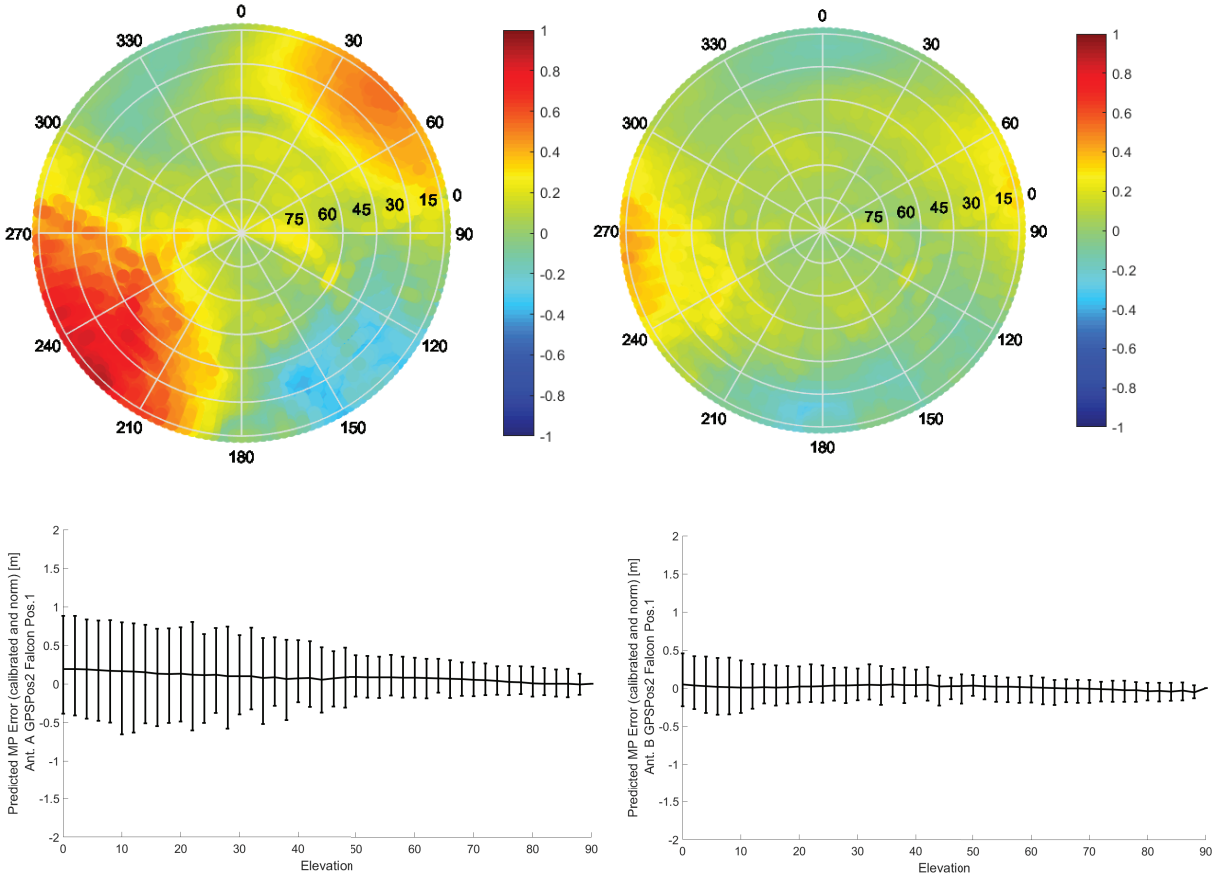

FIGURE 28 Predicted multipath error (in m) as a skyplot (top) or versus elevation (bottom) at the L5 band for Antenna A (left) and Antenna B (right), installed in the GPS Position 1 on a Falcon 200 aircraft

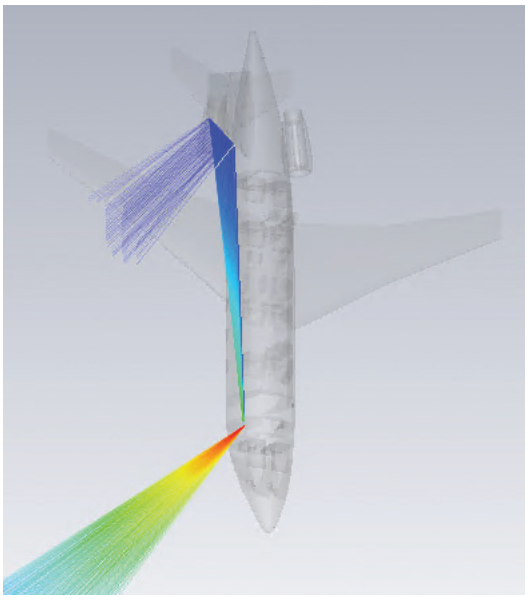

FIGURE 29 Simulation of the rays impinging on the antenna on the Falcon aircraft relative to satellites at an elevation of 80°

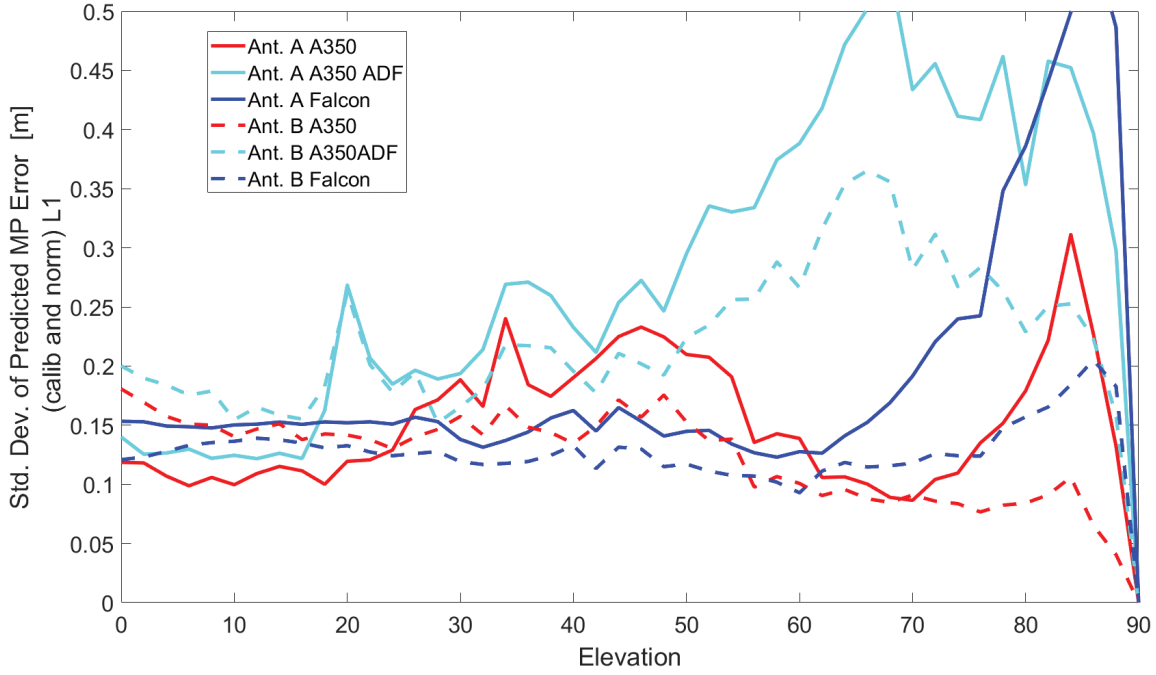

FIGURE 30 Standard deviation of the predicted multipath error (in m, calibrated for antenna-intrinsic pseudorange error and normalized to zenith) at the L1 band for Antennas A and B from the installed performance simulations on an A350 (Position 2 and ADF) and Falcon 200 aircraft

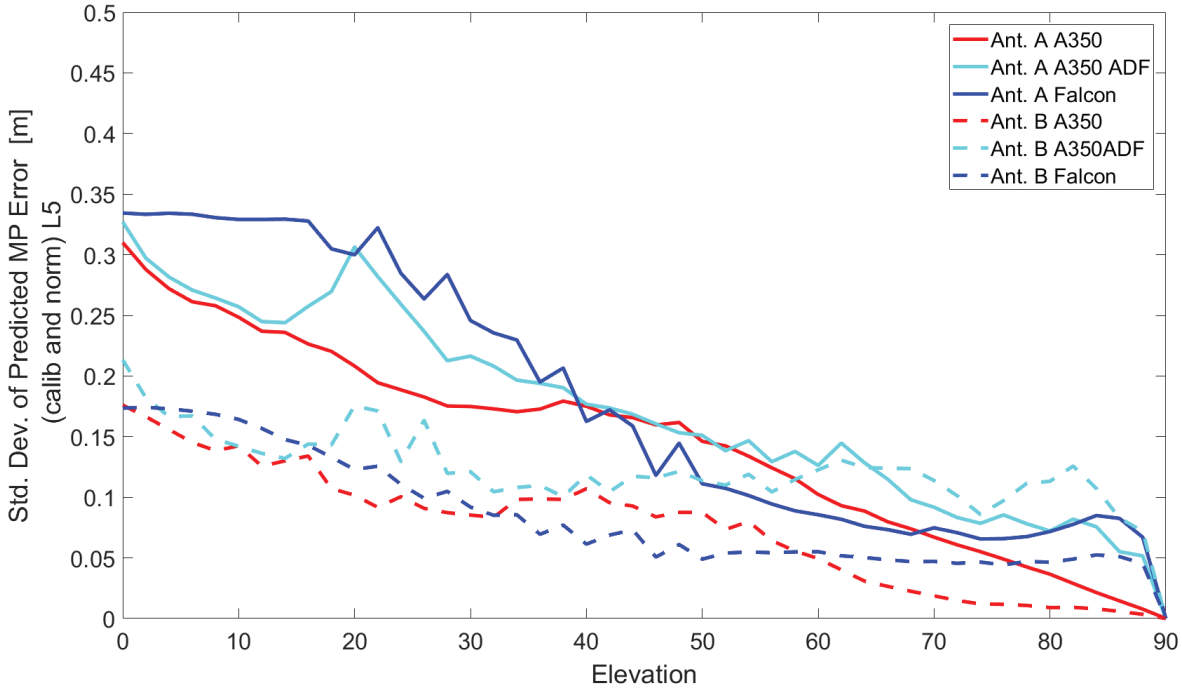

FIGURE 31 Standard deviation of the predicted multipath error (in m, calibrated for antenna-intrinsic pseudorange error and normalized to zenith) at the L5 band for Antennas A and B from the installed performance simulations on an A350 (Position 2 and ADF) and Falcon 200 aircraft

than on that of the L5/E5a, due to the worse MPSR of Antenna A around the zenith at L1. Such an example is relevant for installations in business aviation and/or installations that do not/cannot benefit from the low-multipath environment as in the case of the commercial aircraft.

When calculating the standard deviation values for Falcon and A350 installations, the results in Figure 30 and Figure 31 were found. Indeed, the values obtained with Antenna B were significantly lower than the ones obtained from Antenna A for all elevations, with differences reaching about 20 cm.

4 | TOWARD MULTIPATH MODELS FOR COMMERCIAL AVIATION

The results shown in previous sections have been compared to those obtained by flight data. Overall, a very good agreement was found, validating the simulation approach and also strengthening, on the other side, the validity and correctness of the flight data for the creation of the multipath models.

Figure 32 shows an exemplary comparison of 100-s smoothed multipath root-mean-square (RMS) as obtained by simulation and measurements of data from an A350 aircraft at the L1/E1 band. The measurements-based results were obtained from GNSS observables recorded on the A350 aircraft and then processed to obtain the 100-seconds' smoothed multipath and noise errors with code-minus-carrier techniques (Circiu et al., 2020c). After collecting data from all flights, the estimated errors were then sorted on satellite elevation bins and the RMS for each bin was computed. The satellite elevation refers to the elevation in the level frame (with respect to the horizon).

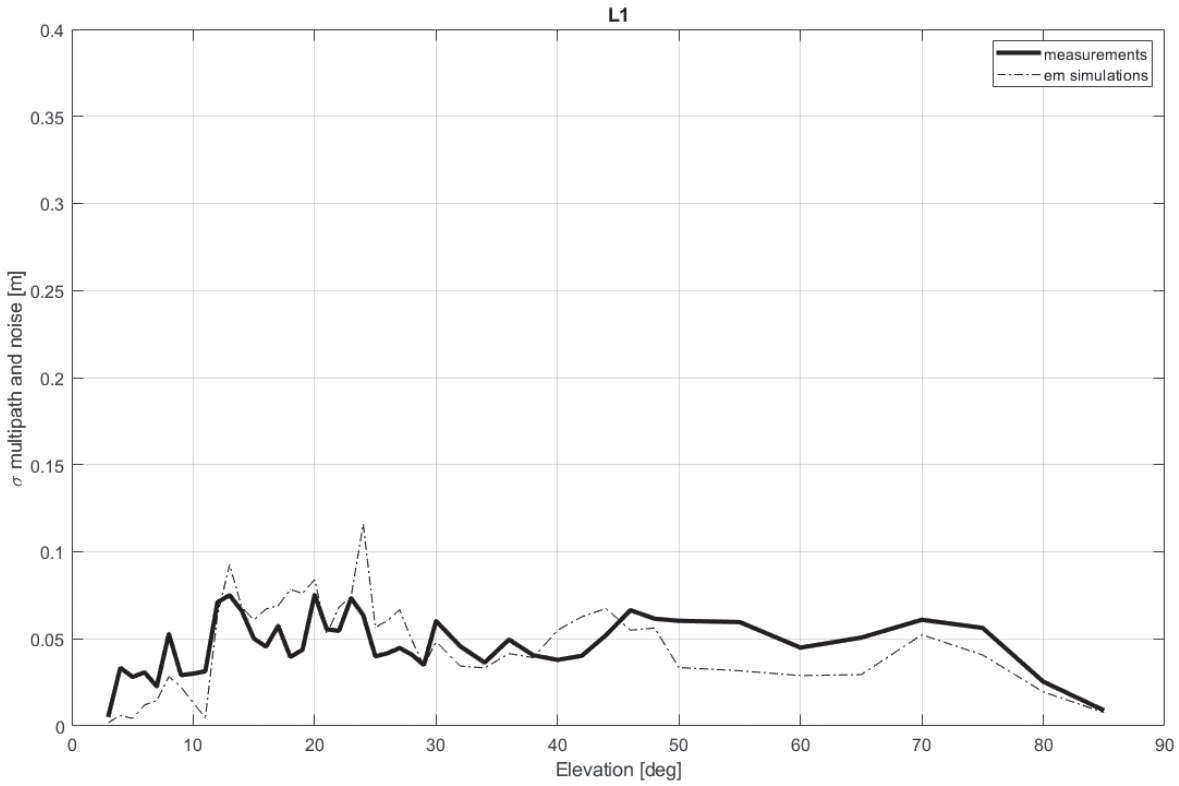

FIGURE 32 Comparison of the 100-s smoothed RMS of the multipath between measurement and simulations for A350 data on the L1 band using Antenna A

The simulation-based results were obtained by mapping the simulated multipath results for the specific aircraft type (available for all azimuth and elevations, but with no time sequence) to the actual angles of arrival for the satellites during the flight campaign to get a sequence of multipath values that could be processed as data from the flight measurement. All the flight trajectories flown on A350 were considered. Based on the satellite elevation and azimuth values at each epoch, the predicted multipath was calculated (i.e., its value for the specific elevation and azimuth was considered) for each epoch, resulting in a time sequence of predicted multipath errors for each satellite. After applying the 100-seconds' smoothing filter, the data was sorted by elevation bin and the RMS of the smoothed predicted multipath was computed for each elevation bin, similar to the measurements-based approach.

For the simulations, the satellite angles were first considered in body-frame and translated into the level frame to be comparable with the measurements-based model and in line with the current defined model. The receiver parameters used were the same as those used in the flight receiver and as specified in Section 2. Antenna A was considered in simulation, as it was the antenna that was actually flown.

The existing residual differences between the two curves (i.e., measured flight data and simulations) could have been caused by a number of effects, including deformation of the aircraft in flight (especially wing flex), the receiver noise (ideal receiver was assumed for simulations), and residual errors from the ionosphere and troposphere, as well as the simplification of the airplane structure in simulation.

Figure 33 shows moreover the raw RMS of multipath obtained using simulation data (using Antenna A) and then evaluated for the satellite geometries obtained during real flights. The big difference between ADF and Position 2 on A350 (as shown already in Figure 30 and Figure 31) is still clearly visible.

However, when performing 100-s smoothing of the results (Figure 34), the difference shrinked consistently due to the capability of the smoothing process to reduce the high-frequency multipath effects.

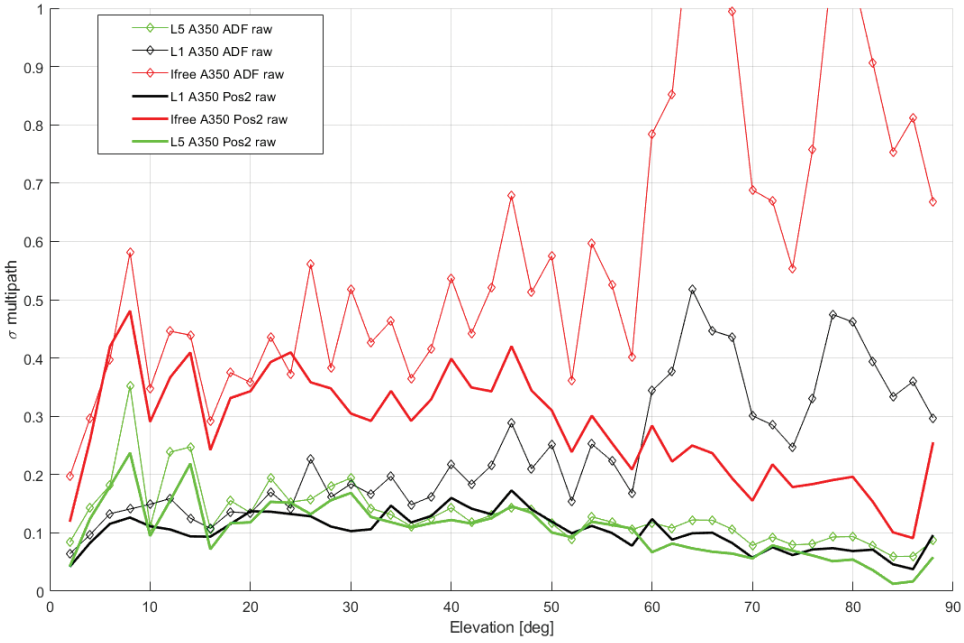

FIGURE 33 Raw RMS of multipath with simulated data from A350 aircraft, processed using the trajectories and satellite constellations seen in real-life flights during the DUFMAN project

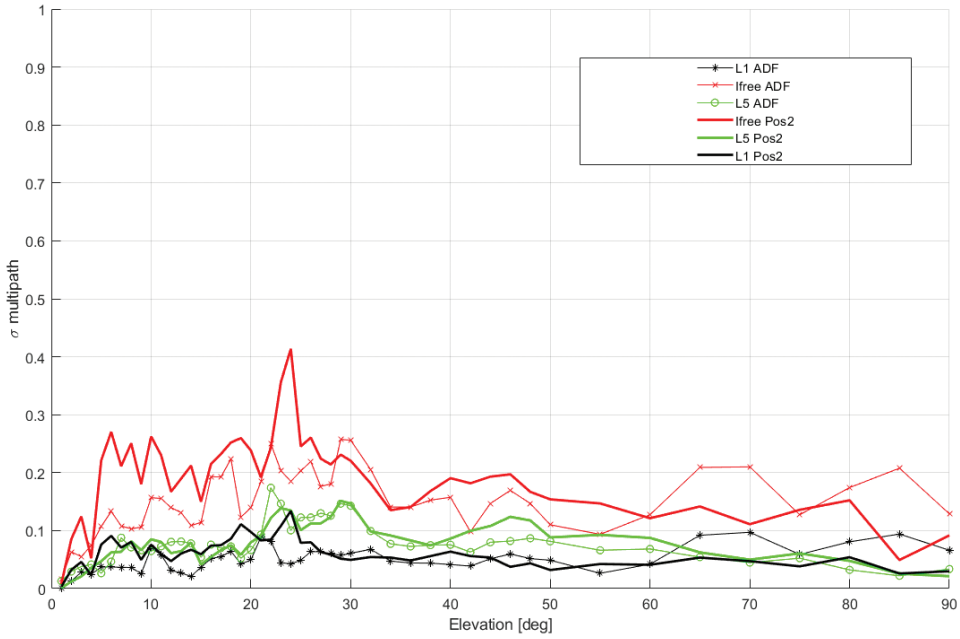

FIGURE 34 100-s smoothed RMS of multipath with simulated data from A350 aircraft processed using the trajectories and satellite constellations seen in real-life flights during the DUFMAN project

This result is important for the practical usability of the multipath models, since it shows that, even in installation points that are moderately scarce from a multipath point of view, the models obtained after 100 seconds of smoothing can be safely used. The validity of this consideration for installations is much more challenging in terms of multipath (for business aviation, helicopters, UAVs, etc.), but it will still need to be investigated and is a topic for future research.

Dual-frequency multi-constellation (DFMC) multipath models have recently been approved by the community based on flight data from the DUFMAN project (Circiu et al., 2020b). Even if data from different aircraft types was analyzed to develop new models, other different installations and antenna positions might need to be taken into account to validate the applicability of the models.

The simulation capability shown here, besides shedding light on the physical phenomena of aircraft multipath, provides the possibility of augmenting the applicability of the models for further installations/aircraft types. Moreover, it provides a basis for the analysis of more complicated installations, as is typical of various avionics platforms such as UAVs, helicopters, and business aviation jets. Further research is, indeed, needed in this respect to evaluate the validity of the current and future multipath models for these avionics platforms.

5 | CONCLUSION

The present paper has brought insight into the role of antennas on pseudorange and multipath errors as experienced in aeronautics. A characterization of different commercial off-the-shelf avionics antennas was performed and indicators for multipath susceptibility have been presented accordingly. Thanks to the integration of electromagnetic measurements and simulations, it was possible to perform a hybrid analysis leading to an estimation of the expected multipath of specific antennas on specific aircraft.

The analysis was then extended to multiple installation points of the antenna on the aircraft and to multiple aircraft types. This estimation method has been shown to agree very well with pseudorange measurement data obtained from flight measurements and can, therefore, be used to augment the current and future development of multipath models by considering installation points and aircraft not flown during the experimentation. The method has agreed with the results obtained from flight data and then flown in the models.

Moreover, open research topics have been identified, such as the need to properly consider the available multipath in avionics platforms other than commercial aviation as well as properly investigating the link between requirements at antenna levels and the achievable performance with respect to pseudorange errors, protection levels, and so on. Further research in this respect is being conducted by the authors and is strongly envisaged by the community.

ACKNOWLEDGEMENTS

Most of the work presented in this paper was carried out in the frame of the project DUFMAN funded by the European Commission (DG-GROW / JRC). Opinions expressed herein are those of the contractor only and do not represent the contracting authorities' official position. The authors would like to thank Airbus for providing the CAD model of the aircraft.

REFERENCES

Amielh, C., Chabory, A., Macabiau, C., & Azoulai, L. (2018). Importance of the antenna model to assess the GNSS multipath in airport environments. *2018 USNC-URSI Radio Science Meeting,* Boston, MA. https://doi.org/10.1109/USNC-URSI.2018.8602861

Appleget, A., & Bartone, C. (2019). A consolidated GNSS multipath analysis considering modern GNSS signals, antenna, installation, and boundary conditions. *Proc. of the 32nd International Technical Meeting of the Satellite Division of the Institute of Navigation (ION GNSS+ 2019).* Miami, FL. https://doi.org/10.33012/2019.16924

Caizzone, S., Circiu, M.-S., Elmarissi, W., Enneking, C., & Winterstein, A. (2019a). Airborne antenna and multipath error characterization for DFMC error standardization. *Proc. of the 32nd International Technical Metting of the Satellite Division of the Institute of Navigation (ION GNSS+ 2019),* Miami, FL. https://doi.org/10.33012/2019.16908

Caizzone, S., Circiu, M.-S., Elmarissi, W., Enneking, C., Felux, M., & Yinusa, K. (2018). Multipath rejection capability analysis of GNSS antennas. *Proc. of the 31st International Technical Meeting of the Satellite Division of the Institute of Navigation (ION GNSS+ 2018),* Portland, OR. https://doi.org/10.33012/2018.16109

Caizzone, S., Circiu, M.-S., Elmarissi, W., Enneking, C., Felux, M., & Yinusa, K. (2019b). Antenna influence on Global Navigation Satellite System pseudorange performance for future aeronautics multifrequency standardization. *NAVIGATION, 66*(1), 99–116. https://doi.org/10.1002/navi.281

Circiu, M.-S., Felux, M., Caizzone, S., Enneking, C., Fohlmeister, F., Rippl, M., Gulie, I., Ruegg, D., Griggs, J., Lazzerini, R., Hagemann, F., Tranchet, F., Bouniol, P., & Sgammini, M. (2020a). Airborne multipath models for dual-constellation dual-frequency aviation applications. *Proc. of the 2020 International Technical Meeting of the Institute of Navigation,* San Diego, CA, 162–173. https://doi.org/10.33012/2020.17135

Circiu, M.-S., Caizzone, S., Felux, M., Enneking, C., Fohlmeister, F., Rippl, M., & Sgammini, M. (2020b). Airborne multipath and antenna error models from the DUFMAN Project. *ICAO Navigation System Panel Meeting*, Montreal.

Circiu, M.-S., Caizzone, S., Felux, M., Enneking, C., Rippl, M., & Meurer, M. (2020c). Development of the dual-frequency dual-constellation airborne multipath models. *NAVIGATION, 67*(1), 61–81. https://doi.org/10.1002/navi.344

Circiu, M.-S., Meurer, M., Felux, M., Gerbeth, D., Thölert, S., Vergara, M., Enneking, C., Sgammini, M., Pullen, S., & Antreich, F. (2017). Evaluation of GPS L5 and Galileo E1 and E5a performance for future multifrequency and multiconstellation GBAS. *NAVIGATION, 64*(1), 149–163. https://doi.org/10.1002/navi.181

Harris, M., Miltner, M., Murphy, T., Raghuvanshi, A., & van Graas, F. (2017). Bounding GPS L1 antenna group delay variations for GNSS landing system integrity. *Proc. of the 2017 International Technical Meeting of the Institute of Navigation,* Monterey, CA, 591–605. https://doi.org/10.33012/2017.14878

Murphy, T., Geren, P., & Pankaskie, T. (2007). GPS antenna group delay variation induced errors in a GNSS based precision approach and landing system. *Proc. of the 20th International Technical Meeting of the Satellite Division of the Institute of Navigation (ION GNSS 2007).* Fort Worth, TX, 2974–2989. https://www.ion.org/publications/abstract.cfm?articleID=7648

Murphy, T., Harris, M., Booth, J., Geren, P., Pankaskie, T., Clark, B., Burns, J., & Urda, T. (2005). Results from the program for the investigation of airborne multipath errors. *Proc. of the 2005 National Technical Meeting of the Institute of Navigation,* San Diego, CA, 153–169. https://www.ion.org/publications/abstract.cfm?articleID=5979

Raghuvanshi, A., & van Graas, F. (2015). Characterization of airborne antenna group delay biases as a function of arrival angle for aircraft precision approach operations. *Proc. of the 28th International Technical Meeting of the Satellite Division of the Insitute of Navigation (ION GNSS+ 2015),* Tampa, FL, 3681–3686. https://www.ion.org/publications/abstract.cfm?articleID=13009

RTCA. (2018). *DO-373: MOPS for GNSS airborne active antenna equipment for the L1/E1 and L5/E5a frequency bands.* RTCA. https://standards.globalspec.com/std/13057420/rtca-do-373

Salabert, F. (2015). Operational benefits of multi constellation dual frequency GNSS for aviation. *Coordinates, XI*(3). https://mycoordinates.org/operational-benefits-of-multi-constellation-dual-frequency-gnss-for-aviation

Van Dierendonck, A., & Erlanson, R. J. (2007). RTCA airborne GPS antenna testing and analysis for a new antenna Minimum Operational Performance Standards (MOPS). *Proc. of the 2007 National Technical Meeting of the Insitute of Navigation,* San Diego, CA, 692–701. https://www.ion.org/publications/abstract.cfm?articleID=7120

Vergara, M., Sgammini, M., Thoelert, S., Enneking, C., Zhu, Y., & Antreich, F. (2016). Tracking error modeling in presence of satellite imperfections. *NAVIGATION, 63*(1), 3–13. https://doi.org/10.1002/navi.129

How to cite this article: Caizzone, S., Circiu, M.-S., Elmarissi, W., Enneking, C., Rippl, M., & Sgammini, M. (2022). The role of antennas on GNSS pseudo-range and multipath errors and their impact on DFMC multipath models for avionics. *NAVIGATION, 69*(3). https://doi.org/10.33012/navi.532